NIST-GCR-97-725

A Burning Rate Model for Charring Materials

Gregory William Anderson

United States Department of Commerce
Technology Administration
National Institute of Standards and Technology

NIST-GCR-97-725

A Burning Rate Model for Charring Materials

Gregory William Anderson

University of Marlyand
College Park, MD 20742

August 1997

U.S. Department of Commerce
William M. Daley, *Secretary*
Technology Administration
Gary Bachula, *Acting Under Secretary for Technology*
National Institute of Standards and Technology
Robert E. Hebner, *Acting Director*

Notice

This report was prepared for the Building and Fire Research Laboratory of the National Institute of Standards and Technology under grant number 60NANB6D0120. The statement and conclusions contained in this report are those of the authors and do not necessarily reflect the views of the National Institute of Standards and Technology or the Building and Fire Research Laboratory.

A BURNING RATE MODEL FOR CHARRING MATERIALS

by

Gregory William Anderson

Thesis submitted to the Faculty of the Graduate School of the
University of Maryland at College Park in partial fulfillment
of the requirements for the degree of
Master of Science
1996

Advisory Committee:

Professor James G. Quintiere
Professor James A. Milke
Professor Jose L. Torero

ABSTRACT

Title of thesis: A BURNING RATE MODEL FOR CHARRING MATERIALS

Degree Candidate: Gregory William Anderson

Degree and year: Master of Science, 1996

Thesis directed by: Professor James Quintiere
Fire Protection Engineering Department

A one dimensional model has been developed to describe the processes involved in the transient pyrolysis of a semi-infinite charring material subjected to a constant radiant heat flux. Material properties are assumed constant with respect to temperature and time. The model tracks the char layer growth, thermal penetration depth, surface temperature and mass loss rate.

A review of the physical phenomena involved in charring pyrolysis is presented and the relevant phenomena included in the model. The integral method is described, and an example for constant surface heat flux is solved. The derivation of the model divides the material into three regions: char layer, vaporization plane, and virgin material and the equations of conservation of mass and energy are applied to each region using the

integral approximation with polynomial temperature profiles. The resulting coupled, nonlinear, autonomous system of three differential equations and one algebraic equation is suitably nondimensionalized and solved using Mathematica™ software. The results generated by the model are compared to existing models and, a method by which effective properties for use in the model might be deduced from experimental data is suggested.

Acknowledgements

I would like to express my indebtedness to my advisor, Professor Dr. James Quintiere for his support throughout this work. Without his advice, suggestions, patience, and corrections this work could not have been completed. I also wish to thank the National Institute of Standards and Technology for their financial support, and the Department of Fire Protection Engineering for allowing me the opportunity to further my education.

TABLE OF CONTENTS

LIST OF TABLES v

LIST OF FIGURES vi

Chapter 1-- Introduction 1
Background 1
Previous work 3
Delichatsios and deRis 3
Chen 4
Wichman and Atreya 4
Suuberg, Milosavljavik, and Lilly 5
Kashiwagi, Ohlemiller, and Werner 5
Overview of thesis 5

Chapter 2 — Pyrolysis 7
Introduction 7
Qualitative phenomena 7
Simplifying Assumptions 9
Conclusions 10

Chapter 3 -- Integral Method 11
Introduction 11
Explanation of method 12
Example: Semi-infinite solid & constant surface flux 13
Conclusions 17

Chapter 4 -- Pyrolysis Model 18
Introduction 18
Assumptions 18
Conservation equations 20
Conservation of Mass 21
Conservation of Energy 21
Vaporization plane 23
Conservation of mass 23
Temperature profile 25
Conservation of energy 25
Virgin material 27
Conservation of mass 27
Temperature Profile 28
Conservation of Energy 29

Char 30
Conservation of mass 30
Temperature Profile 31
Conservation of energy 32
Conclusions 33

Chapter 5 -- Solving the Model 35
Introduction 35
Dimensional Analysis 35
Composite parameters 35
Dimensionless groups 36
Independent Variables 36
Dependant Variables 37
Problem Parameters 38
Dimensionless form of the equations 39
Solving the equations 39
Initial Conditions 40
Series Solution 41
Solution method 42
Conclusion 44

Chapter 6 -- Model results 46
Introduction 46
Delichatsios and deRis 46
Chen 49
Ohlemiller, Kashiwagi, and Werner 53
Conclusions 60

Chapter 7 -- Applications of the model 61
Introduction 61
Small time ($\tau \approx \tau_{ig}$) 61
Long Time ($\tau >> \tau_{ig}$) 64
Implementing the approach 66
Conclusion 70

Chapter 8 -- Conclusions 71

Appendix I -- Mathematica Routine 73

NOMENCLATURE 78

REFERENCES 81

LIST OF TABLES

Table		Page
Table 1	Properties for Delichatsios and de Ris comparisons	49
Table 2	Properties used in the Chen Comparisons	53
Table 3	Property values used in Ohlemiller Comparisons	55
Table 4	Properties used in the demonstration of the application	69

LIST OF FIGURES

Figure		Page
Figure 1	Schematic for integral method	13
Figure 2	Comparing the Integral approximation to the exact solution	17
Figure 3	Charring material	19
Figure 4	Control volume surrounding the vaporization plane	23
Figure 5	Control volume surrounding the virgin material	27
Figure 6	Control volume enclosing the char layer	30
Figure 7	Comparison against Delichatsios and de Ris	47
Figure 8	Re-scaled plot of deRis vs. the current model	48
Figure 9	Comparison of mass loss rates (Chen and current)	50
Figure 10	Plot focussing on the peak behavior (Chen and current)	51
Figure 11	Comparison to Chen for constant thermal conductivity.	52
Figure 12	Comparison of mass loss in inert and oxygenated atmospheres	54
Figure 13	Base case for 25 kW/m^2 vs. Ohlemiller	56
Figure 14	Base case for 40 kW/m^2 vs. Ohlemiller	56
Figure 15	Base case for 70 kW/m^2 vs. Ohlemiller	57
Figure 16	Effects of varying L for 40 kW/m^2	58
Figure 17	Effect of varying T_v for 40 kW/m^2	59
Figure 18	Effect of varying ϵ for the 40 kW/m^2 case	59
Figure 19	Comparing the short and long time approximations	67
Figure 20	Compare approximations against model predictions	68
Figure 21	Comparing the corrected long time approximation to the predicted peak	69

Chapter 1– Introduction

Background

Engineering has been described as:

> *The practice of designing structures we cannot completely describe, out of materials we do not completely understand, to withstand loads we cannot completely predict, without ever letting anyone know how ignorant we really are.*

In fire protection engineering this statement is often uncomfortably true. Fire protection engineers frequently assess the fire hazard of a building or other structure, using information about the expected building contents and the conditions the building can be expected to experience. The engineer analyzes this information using models based on physical laws and develops some judgement as to the degree to which the building can be considered "safe." In some scenarios, the engineer can predict the response with good confidence, in others with fair confidence, and in still others with poor confidence.

The problem of determining the fire hazard posed by the materials within the building generally falls into the second or, occasionally, even the third category. Computer models do exist to assist the engineer, but the current state of the art imposes some severe restrictions. Rather than specify a plausible ignition source and use the model to predict the subsequent growth of the fire, current models require the engineer to specify the growth of the fire, which is often part of the aim of applying the model in the first place. The reason for this is straightforward: no simple, universally accepted model exists to predict the behavior of general materials under fire conditions.

Modelling the behavior of solid materials as they pyrolyse under fire conditions is an extremely challenging task. There are many physical phenomena that come into play, and determining how these phenomena interact is daunting at best. Engineers must make assumptions regarding the nature of the phenomena and their interactions.

The rate at which materials pyrolyse is a key factor in determining the hazard. On the fire triangle, (of heat, fuel, and oxygen), the pyrolysis rate determines the available fuel. To a lesser extent, the pyrolysis rate also determines the heat, since the heat generated in the fire can be modelled as the product of the heat of combustion and the mass of fuel burned. Also, a material that does not pyrolyse readily may absorb substantial energy, leaving less available to ignite nearby objects

Solid materials can be classified by their pyrolysis behavior into two basic categories: non-charring and charring. Non-charring materials burn away completely, leaving little to no residue. Charring materials, on the other hand, do not burn away completely, leaving behind (relatively) substantial amounts of residue. Non-charring materials can be modelled using theory similar to flammable liquids, with surface pyrolysis, a constant surface temperature, and a steady state condition. Charring materials must be modelled by a pyrolysis front penetrating into the material, an increasing surface temperature, and without a well-defined steady state. The bulk of this work considers only charring materials.

Previous work

Various approaches to modelling charring pyrolysis have been developed, and several relevant studies will be reviewed before continuing on the current work. In the interest of space, only a few of the many studies will be specifically mentioned.

Quintiere[17] presented an approach to modelling the burning rate of solid materials. He formulates a general model valid for both charring and non-charring materials by applying the conservation of mass and energy to regions of the material. The current model employs his method to derive the governing equations for charring materials and solves them. Iqbal[11] previously developed and solved the governing equations for non-charring materials.

Delichatsios and deRis [5] developed a one dimensional analytical model for charring pyrolysis. They assume a semi-infinite fuel bed subjected to a constant external radiative heat flux, neglecting convective effects. They also neglect the thermal capacity of both the pyrolysed gases and the residual char matrix. They assume that pyrolysis occurs in a narrow region, at fixed temperature, and with a constant heat of gasification. Their model focusses on the pyrolysis process without a flame. They develop their model from the conservation of energy equation and its first moment, assuming an exponentially decaying temperature profile within both the char layer and virgin material. They model conduction through the solid using a radiative interstitial model, which provides a variable conduction rate. Their model describes the behavior

of the pyrolysis rate for relatively large times, after the initial transient peak. Their primary finding was that the pyrolysis rate falls off as $1/\sqrt{t}$.

Chen[2] also developed a one dimensional model for charring pyrolysis. His model, for material of finite thickness and constant properties exposed to a constant radiative incident heat flux, assumes that pyrolysis occurs in a narrow region, at constant temperature, and with constant heat of gasification. Like Delichatsios and deRis, he used the energy equation and its first moment for both the virgin material and char layer, assuming (different) exponential temperature profiles in each. Chen developed the model to treat strictly pyrolysis, ie. no flame, and to consider the entire time of exposure -- from heat up to initial pyrolysis to thick char. His results indicate that the mass loss rate increases to a peak value shortly after the start of heating, and falls off from there, at a rate asymptotically approaching that shown by Delichatsios and deRis, $1/\sqrt{t}$.

Wichman and Atreya[22] present a slightly more involved one dimensional pyrolysis model. They make the assumptions of a semi-infinite fuel bed, constant properties, negligible interaction between the volatile gases and the char matrix, and negligible heat of pyrolysis. They model the pyrolysis process itself using a single step chemical reaction. Their model breaks the time period into four general regions: an inert heating period, a short transition regime, a thin char period, and a thick char region. Their results suggest that pyrolysis initially behaves in a wavelike way and that

the thickness of the reaction zone increases as $\sqrt{t}$, so therefore the assumption of an infinitesimally thin reaction zone degrades for large time.

Suuberg, Milosavljavik, and Lilly[19] present an extremely detailed model for the one dimensional pyrolysis process. This work is composed of both experimental work and theoretical modelling. Their experimental work provides a great deal of insight into the physical phenomena involved in pyrolysis. Their mathematical model is one dimensional, for an infinite slab geometry. They assume that properties are a function both of temperature and of the fraction of virgin material and pyrolysate. Pyrolysis is modelled by finite rate chemistry, and includes the heat of pyrolysis. Radiation effects include variable emissivity and reflectivity. Their work indicates that chemical kinetics are important, but also that there are two separate kinetic regimes that must be included. They also find that the assumption of an infinitesimal pyrolysis zone is valid for incident heat flux greater than 40 kW/m^2.

Kashiwagi, Ohlemiller, and Werner[14] performed experiments to study the pollutants generated in wood burning stoves. In doing so, they heated wood samples (chiefly white pine and red oak) without flaming using uniform radiant heat fluxes varying from 2 to 7.8 W/cm^2. In addition to monitoring or trapping several species of products, they reported either sample temperature or mass loss rate for each test

Overview of thesis

Chapter Two contains a detailed description of the pyrolysis. In this chapter, most of the physical phenomena involved are described, and quantitative relationships

describing those considered relevant are given. Chapter Three contains a brief description of the integral method used to derive the current model. Here the case of a semi-infinite material exposed to a constant radiative flux is solved using the integral approach and compared with an exact solution. Chapter Four explains the derivation of the current model. Chapter Five presents the non-dimensional groups used in simplifying the governing equations, and describes the solution method. Chapter Six compares results from the current model against results from other models. Chapter Seven outlines a method by which the current model can be compared to experimental data and effective properties for use in the model might be deduced. Chapter Eight summarizes the conclusions of this work, and makes some suggestions for future work.

Chapter 2 — Pyrolysis

Introduction

The first step in modelling is formulation. A material undergoing pyrolysis involves a large number of individual phenomena. This chapter attempts to present many of these processes and their relative importance, both within the current model and in the overall scheme of things. Chapter Four will complete the formulations step. For more thorough discussions, the interested reader is referred to the references.

Qualitative phenomena

First, consider materials under ambient conditions. Assuming thermodynamic equilibrium, the material has a uniform temperature distribution equal to that of the surroundings. In addition, most materials have absorbed (by virtue of the humidity of their surroundings) some small quantity of water. Finally, most materials undergo a slow, continuous degradation process; a chemical reaction that proceeds at an insignificant pace under ambient conditions.

Now, consider that this material has been subjected to an external heat source. As the applied heat is conducted through the material, a thermal wave front forms and advances into the material. As the temperature of the material rises, the absorbed water (which had been in equilibrium) vaporizes at an increasing rate, absorbing some of the conducted energy. This vaporization process prevents the material temperature from exceeding the saturation temperature of the absorbed water. The production of water vapor develops a pressure distribution within the material that drives a fraction of

the vapor out of the material and the remaining vapor into the unaffected material. Once all of the water has vaporized, the internal temperature again begins to rise. As the material temperature rises, the degradation reactions accelerate until a critical temperature is reached. At this temperature, the rate of reaction steeply increases and the leading edge of a pyrolysis zone develops.

Within this zone the material breaks down. Charring materials tend to be mixtures, with each component decomposing at different temperatures and into different materials (non-charring materials tend to be homogenous). The char develops because the lighter, more volatile materials vaporize first, leaving behind the denser components. These less reactive components remain behind and may decompose more rapidly as the temperature continues to rise. The least reactive components form a brittle matrix that is the char. The volatile gases generated by pyrolysis accumulate, augmenting the pressure distribution developed by the water vapor. The volatiles, like the water vapor, are driven both deeper into the unreacted material as well as toward the surface. The volatiles driven into the material cool and condense, only to be revaporized when the pyrolysis front penetrates further. The char matrix is usually much more brittle than the virgin material and is easily fractured by the internal pressure gradient, allowing the pyrolysate to escape.

As the char layer grows, it acts in several ways to diminish the pyrolysis process. First, it acts as an insulator, inhibiting the conduction of heat to the pyrolysis zone and thus decreasing the pyrolysis rate. Second, the char can absorb energy and

increase in temperature. The surface temperature rises, and re-rediation losses increase dramatically. After a sufficiently long exposure, these effects inhibit the conduction to such a degree that pyrolysis effectively ceases.

Simplifying Assumptions

Having discussed many of the phenomena of charring pyrolysis, it is obvious that many simplifying assumptions should be considered. These simplifications will be considered here in a qualitative way, and in the next chapter they will be more rigorously developed.

First, consider the ambient conditions. The temperature within the material has a uniform distribution T_0. In addition, while it is true that there will likely be some absorbed water, to simplify the current analysis this water is assumed to be negligible. Finally, the degradation process is a chemical reaction, generally assumed to be described by a single step, first order, Arrhenious rate equation:

$$\frac{d\rho}{dt} = -Ae^{-E/RT} \qquad (1)$$

A is the Arrhenious factor, or rate constant; E is the activation energy for the reaction; R is the universal gas constant; and T is the temperature at which the reaction occurs.

Next consider the effects of an external heat source on the material. As the material absorbs energy, the temperature rises, and the properties begin to change. This change is small, and so properties can be evaluated for an average temperature and assumed constant throughout the process. As the temperature rises, the reaction rate

given by equation 1 increases exponentially. Because it increases exponentially, there is some point where the rate skyrockets, and the reaction can be considered to proceed instantaneously. Infinite rate chemistry implies that the reaction occurs over a thin region. This is the assumption used in the current model. According to Suuberg[19], this will be valid for imposed heat fluxes greater than 40 kW/m^2. Wichman and Atreya[22] also suggest that the reaction zone broadens over time, and so the validity of the assumption degrades over time. Nevertheless, for fire conditions, it is hoped that this assumption will be accurate enough.

Finally, consider the interaction between the volatiles and the char. The char matrix is brittle, so even a small pressure gradient will quickly fracture it. In addition, the char layer is thin, so transport time from the pyrolysis zone to the surface will be short. The volatiles can probably be assumed to immediately exit the material as they are generated. The paths the volatiles take through the matrix are extremely thin, so heat transfer between the volatiles and char will take place quickly. Therefore, the respective temperatures are assumed equal throughout the char layer.

Conclusions

In this chapter, phenomena known to occur during charring pyrolysis were presented. Inclusion of all listed phenomena would result in a model too complicated for easy application, so reasonable approximations were developed. In the next chapter, these assumptions will be further developed analytically.

Chapter 3 – Integral Method

Introduction

The full partial differential equation form of the heat equation is challenging to solve exactly, particularly when there exist inhomogeneities such as heat generation or consumption terms. Solving the equation exactly requires certain types of boundary conditions, and these are not always found in practice. Even if the solution can be determined, it is often too complicated for easy application.

Fortunately, there is an alternative. The approximate integral method provides a way to derive a solution to a nonlinear, transient heat conduction problem. In solving the equation exactly, the temperature distribution within the material is determined such that the heat equation is exactly satisfied for each differential element. In the approximate integral method, the shape of the temperature distribution is assumed, and relevant parameters are determined in such a way to fit the boundary conditions and satisfy the equation for the average over the region. This method is relatively insensitive to the exact character of the assumed profile, whether it be quadratic, cubic, quartic, exponential, etc.[15] This method is also quite flexible by admitting solutions for many boundary conditions.

In this chapter, the integral approximation will be explained and applied to a sample case relevant to this thesis. The charring problem under consideration is formulated as a semi-infinite solid subjected to a constant heat flux at the surface. Here, an analysis of this case will be conducted assuming a quadratic polynomial

temperature distribution. The results of this analysis will be compared with an exact solution.

Explanation of method

The approximate integral method was first applied to transient heat transfer problems in 1958 by Goodman, and the current presentation follows that of Özişik[15]. The method consists of four steps: assume a temperature profile, integrate over the thermal layer, solve the resulting ordinary differential equation, and substitute into the profile.

The first step is to assume a temperature profile. Polynomial profiles are commonly assumed, but the method is valid for exponential or trigonometric profiles as well. The boundary conditions are used to determine the unknown coefficients in the profile, so one might choose a quadratic polynomial with three unknowns to satisfy three boundary conditions. In this case, $T(x, t)=A(t)+ B(t)x+C(t) x^2$. The time dependance of the coefficients arises from a characteristic length $\delta(t)$. This length, the thermal layer, represents the extent to which the applied boundary conditions have affected the material at time *t*, and will typically increase over time. Note that the introduction of this thermal length may introduce additional boundary conditions. For example, for a semi-infinite material, at $\delta(t)$ the temperature is that of the unaffected material, and there is no heat conduction $-k\frac{dT}{dx}\Big|_{x=\delta} = 0$.

The second step is integrating over the thermal layer. Both sides of the partial differential equation are integrated once with respect to the spacial variable over the

characteristic length $\delta(t)$. The values at the limits of integration are supplied by the boundary conditions. This integration will reduce the partial differential equation in x and t to a first order ordinary differential equation in t.

The third step is to solve the ordinary differential equation. Commonly, the initial condition $\delta(0)=0$ is used, although in some multi-step problems other initial conditions might be used if appropriate.

The fourth (and final) step is to substitute the solution to the differential equation back into the profile. This provides the time dependance for the profile.

Example: Semi-infinite solid & constant surface flux

Consider a semi-infinite solid at a uniform temperature T_0. At time t=0, the material is suddenly subjected to a constant radiant heat flux, uniform over its surface. A general schematic for this is given in figure 1.

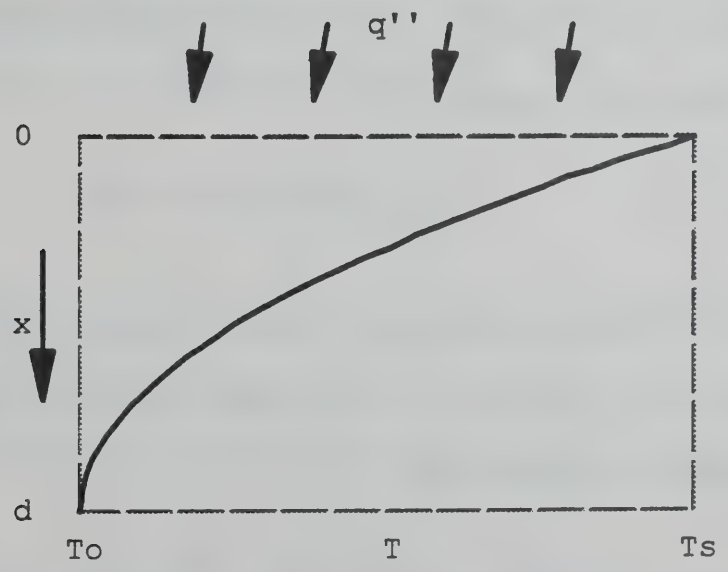

Figure 1 Schematic for integral method

The subsequent evolution of the material temperature is governed by the relationship:

$$\rho c \frac{\partial T}{\partial t} = k \frac{\partial^2 T}{\partial x^2} \qquad (2)$$

Subject to the boundary conditions:

$$\dot{q}'' = -k \left.\frac{\partial T}{\partial x}\right|_{x=0} \text{ (a)} \qquad 0 = -k \left.\frac{\partial T}{\partial x}\right|_{x=\delta(t)} \text{ (b)} \qquad T(\delta(t),t)=T_0 \text{ (c)} \qquad (3)$$

Here $\delta(t)$ represents the depth of penetration of the thermal wave, labeled as d in figure 1. For $x<\delta$, the temperature has risen from the initial value; for $x \geq \delta$, the temperature remains undisturbed at the initial value.

To apply the integral approximation, a profile must first be chosen. Since there are three boundary conditions, there must be three unknowns in the profile. Therefore, for this analysis use a quadratic in x:

$$T(x,t) = A(t)x^2 + B(t)x + C(t) \qquad (4)$$

The idea of the integral method is to use equation 4 together with the boundary conditions 3(a-c) to solve for the time dependant coefficients A(t), B(t), C(t). Solving appropriately, the coefficients are:

$$A(t) = \frac{\dot{q}''}{2k\delta(t)} \text{ (a)} \qquad B(t) = -\frac{\dot{q}''}{k} \text{ (b)} \qquad C(t) = T_0 + \frac{\dot{q}''\delta(t)}{2k} \text{ (c)} \qquad (5)$$

Substituting into equation 4 and simplifying, the profile takes the form:

$$T(x,t) - T_0 = \frac{\dot{q}''\delta(t)}{2k}\left(1 - \frac{x}{\delta(t)}\right)^2 \qquad (6)$$

Now that the profile has been assumed, the analysis continues to the next step: using the assumed profile to transform the heat equation (a partial differential equation) into an ordinary differential equation.

The analysis proceeds by integrating equation 2 over the affected region $0 \leq x \leq \delta(t)$. This integration yields

$$\rho c \frac{d}{dt}\int_0^{\delta(t)} (T(x,t) - T_0)dx = -k\left.\frac{dT}{dx}\right|_{x=0} = \dot{q}'' \qquad (7)$$

Substituting the assumed profile 6 into equation 7 and evaluating the integral and derivative produces an ordinary differential equation

$$\frac{d\delta}{dt} = \frac{3\frac{k}{\rho c}}{\delta} \qquad (8)$$

which can be easily solved to give the penetration depth $\delta(t)$

$$\delta(t) = \sqrt{6\alpha t} \quad \text{where } \alpha = \frac{k}{\rho c} \qquad (9)$$

This expression for δ(t) and be substituted into equation 6 to give the overall expression for the profile within the material:

$$T(x,t) - T_0 = \frac{\dot{q}''\sqrt{6\alpha t}}{2k}\left(1 - \frac{y}{\sqrt{6\alpha t}}\right)^2 \qquad (10)$$

The exact solution, given by Incropera and DeWitt [11] is:

$$T(x,t) - T_0 = \frac{\dot{q}''\sqrt{\frac{16}{\pi}\alpha t}}{2k}\exp\left(-\frac{x^2}{4\alpha t}\right) - \frac{\dot{q}''x}{k}\operatorname{erfc}\left(\frac{x}{\sqrt{4\alpha t}}\right) \qquad (11)$$

A suitable choice of non-dimensional variables would simplify these equations. Making the substitutions

$$T^* = \frac{T(x,t) - T_0}{\frac{\dot{q}''}{k}\sqrt{\alpha t}} \quad (a) \qquad x^* = \frac{x}{\sqrt{\alpha t}} \quad (b) \qquad (12)$$

the integral approximation (equation 10) can be simplified to

$$T^* = \sqrt{6}\left(1 - \frac{x^*}{\sqrt{6}}\right)^2 \qquad (13)$$

and the exact answer (equation 11) reduces to

$$T^* = \frac{4}{\sqrt{\pi}}\exp\left(-\left(\frac{x^*}{2}\right)^2\right) - x^*\operatorname{erfc}\left(\frac{x^*}{2}\right) \qquad (14)$$

These two equations are compared in figure 2, below.

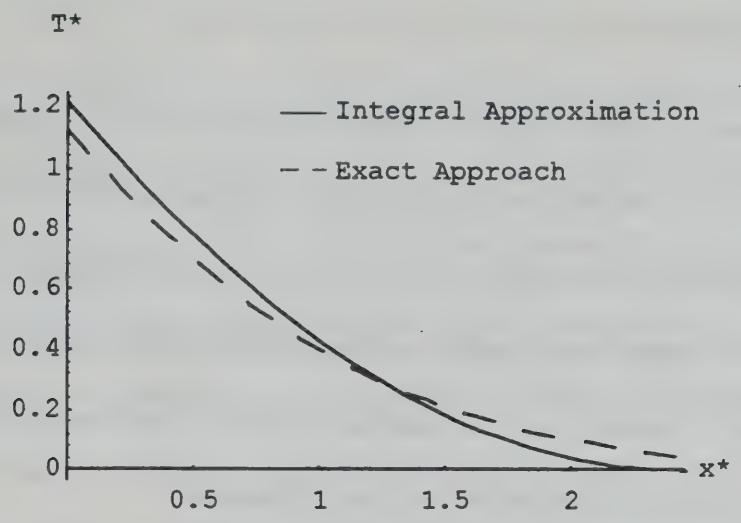

Figure 2 Comparing the Integral approximation to the exact solution

The solid line represents the approximation, and the dashed line represents the exact solution. This figure shows the good agreement between the approximate method and the exact solution although the exact solution never quite reaches zero.

Conclusions

The approximate integral method is a powerful tool in solving transient heat transfer problems. In this chapter the method was explained and applied to the case of a semi-infinite material exposed to a constant radiant heat flux. The exact solution to this problem is known, and the approximate method compares well against it. This method (and in fact the test case presented here) is used heavily in the current model.

Chapter 4 – Pyrolysis Model

Introduction

This chapter completes the formulation of the model of the model introduced in Chapter Two. First, the basic assumptions fundamental to the model are recounted, followed by a brief discussion of the form of conservation of mass and energy used. The conservation equations are applied to the material, and the governing equations are derived. Then, by choosing suitable dimensionless groups, the forms of the equations are simplified. Finally the method of solution is presented.

Assumptions

The following theory is based on a number of physical assumptions developed and justified in Chapter Two. For convenience they are repeated here. The material is modelled as semi-infinite; that is, having one defined surface and otherwise extending to infinity in all directions. The material properties (thermal conductivity, density, specific heat, etc.) are constant over the range of temperatures considered. Pyrolysis begins instantly when the temperature reaches the pyrolysis temperature, and proceeds to completion instantly. Pyrolysis requires a fixed energy (heat of gasification). Vaporization takes place in a region of infinitesimal thickness that advances into the material. The pyrolysed gases do not accumulate within the char matrix; all volatiles produced exit the material immediately.

The material is divided into three regions. A diagram is shown in figure 3. The bottom region is the virgin material. This is the unreacted material affected by the

boundary conditions. In this region the temperature profile is parabolic and the material properties are considered those of the unreacted material. The top layer is the char. The char is the residue that remains after the pyrolysis reaction is completed. In this region the temperature profile is linear and the thermodynamic properties are those of the residual char. The vaporization plane separates the virgin material from the char. Here the virgin material pyrolyses into volatile gases and char. In this plane the temperature is constant at T_v and pyrolysis consumes a fixed energy ΔH_v. There is a fourth region, the substrate, under the virgin material (not shown). The substrate is the virgin material that has not yet been affected by the boundary conditions. In this region the temperature profile is uniform at T_0 and the thermodynamic properties are those of the unreacted material. The substrate is omitted from further consideration because nothing of interest happens in that layer.

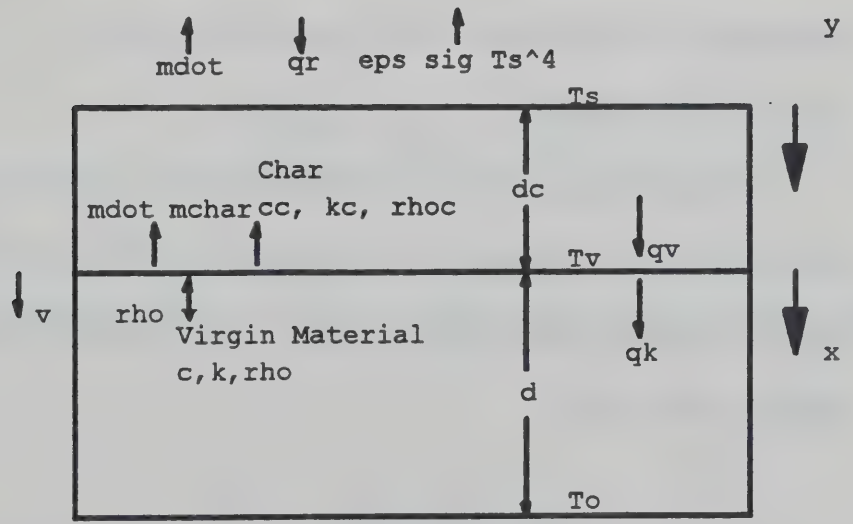

Figure 3 Charring material

In the following sections, mass and energy balances are considered for the vaporization plane, the virgin material, and the char.

The model is developed for the following case. The material is first in thermodynamic equilibrium with the environment. At time t=0 it is subjected to an imposed radiant heat flux q_r''. This is considered to be the actual flux absorbed by the material, i.e., the absorbtivity is assumed constant and included in the flux term. A temperature profile begins to develop, defining the virgin material region. The transient development in this phase is identical to the analysis in Chapter Three. At some time $t=t_{ig}$ the surface temperature reaches the pyrolysis temperature, T_v, the vaporization plane forms and pyrolysis begins. The vaporization plane travels into the material, breaking it down into volatile gases and residue. The gases escape the material, and the residue left behind defines the char layer. The current model treats the evolution of the char process from the initiation of the vaporization plane $t=t_{ig}$.

Conservation equations

The governing equations for the current model are derived by applying the conservation of mass and energy to control volumes enclosing each of the three regions vaporization plane, virgin material, and char. Here the relevant forms of these principles are developed.

Conservation of Mass

The principle of conservation of mass (continuity) states that the rate of mass storage is equal to the difference between the rate mass enters and leaves the boundaries of the control volume.

$$\frac{dm_{stored}}{dt} = \dot{m}_{gained} - \dot{m}_{lost} \tag{15}$$

Conservation of Energy

The principle of conservation of energy (first law of thermodynamics) states energy can neither be created nor destroyed, merely changed from one form to another. For the purposes of this work, this means that the rate of accumulation of energy within the control volume equals the difference between the rates of energy loss and gain.

$$\frac{dE_{stored}}{dt} = (\dot{E}_{gained} - \dot{E}_{lost}) \tag{16}$$

Using the definition of internal energy, the stored energy can be calculated by the relation

$$E_{stored} = \int_V \rho \left(\int_{T_0}^{T} c\,dT \right) dV \tag{17}$$

Since the temperature distribution within the material is known and assuming constant properties and one dimensional behavior, this expression can be rewritten as

$$E_{stored} = \rho c \int_0^y (T - T_0) dy \tag{18}$$

The control volumes can gain or lose energy by conduction, convection, or radiation. Where conduction is indicated, it is assumed to follow Fourier's law of conduction, given by:

$$\dot{q}'' = -k \frac{\partial T(x,t)}{\partial x}\bigg|_{x=x_0} \tag{19}$$

where $\dot{q}''$ is the heat flux, T(x, t) is the assumed profile, and $x=x_0$ is the point of interest. Convection takes place where mass crosses the boundary of the control volume. Where this is indicated, the enthalpy flow rate is given by $\dot{m}_n''Ah_n(T)$, where h_n (T) represents the enthalpy possessed by species *n* at temperature T, defined as:

$$h_n(T) \equiv \int_{T_0}^{T} c_{p_n}(T) dT \tag{20}$$

Obviously, if the specific heat, $c_{p,n}(T)$, is constant, this reduces to

$$h_n(T) \equiv c_{p_n}(T - T_0) \tag{21}$$

Finally, energy radiated from a control volume follows the Stefan-Boltzmann equation and is given by:

$$\dot{q}'' = \epsilon \sigma T^4 \qquad (22)$$

where ϵ is the emissivity and σ is the Stefan-Boltzmann constant (σ=5.67 10^{-8} W/m^{2}K^4)

Vaporization plane

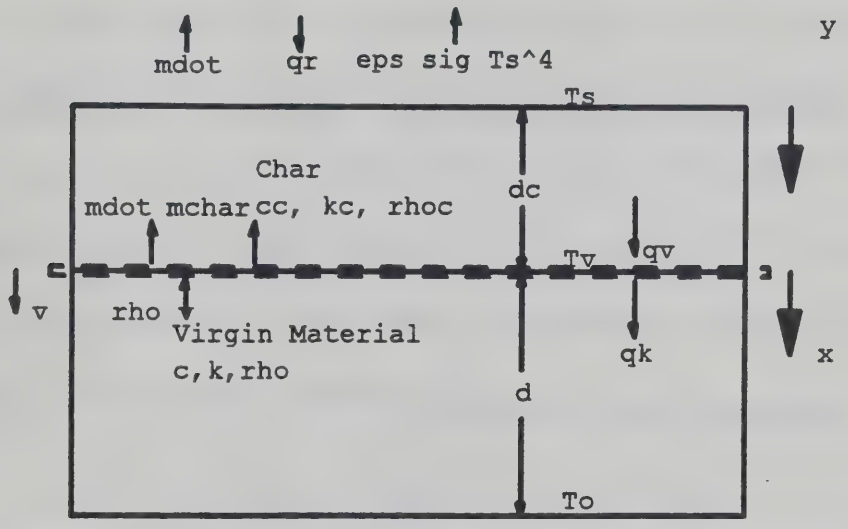

Figure 4 Control volume surrounding the vaporization plane

Conservation of mass

The first region to be studied is the vaporization plane. As a plane, this region has an infinitesimal thickness so the volume, and consequently the mass, is zero. However, a mass balance can be written for the control volume enclosing the plane. The control volume is shown in figure 4. The control volume gains mass as the plane advances into the virgin material and loses mass as the pyrolysis process breaks the

material into char and volatiles. The infinitesimal thickness means that no mass is stored, and so the mass gained equals the mass lost. This is expressed as

$$\rho v A = (\dot{m}_c'' + \dot{m}'')A \tag{23}$$

Using $\dot{m}''_c = \rho_c v$ and $\phi = \rho_c/\rho$, equation 23 can be rewritten as

$$\rho v = \frac{\dot{m}''}{(1-\phi)} \tag{24}$$

The speed of the vaporization plane, v, is also the rate at which the char layer grows,

$$v = \frac{d\delta_c}{dt} \tag{25}$$

so equation 24 can be rewritten as:

$$\frac{d\delta_c}{dt} = \frac{\dot{m}''}{\rho(1-\phi)} \tag{26}$$

Alternately, an expression in terms of $\dot{m}_c''$ can be derived from equation 23 as follows

$$\dot{m}_c'' = \frac{\phi \dot{m}''}{(1-\phi)} \tag{27}$$

Temperature profile

The vaporization plane represents the pyrolysis zone and the pyrolysis process is assumed to take place at a fixed temperature, T_v. Therefore, the temperature profile for the vaporization plane is the single, constant temperature T_v.

Conservation of energy

Consider an energy balance on the control volume enclosing the vaporization plane. Since it contains no mass, no energy can be stored. The endothermic nature of pyrolysis will be accounted for below. Examining figure 4, the control volume gains energy two ways: by heat conduction from the char layer, $\dot{q}_v''$, and by enthalpy possessed by the mass entering the control volume, $\rho v A h_v(T_v)$. The control volume loses energy two ways: heat conduction into the virgin layer, $\dot{q}_k''$, and by enthalpy possessed by the char and volatiles left behind by the vaporization plane, $\dot{m}_c'' A h_c(T_v)$ and $\dot{m}'' A h_g(T_v)$. Expressing this mathematically:

$$\rho v h_v A(T_v) - A\left(\dot{m}_c'' h_c(T_v) + \dot{m}'' h_g(T_v)\right) = \dot{q}_k'' A - \dot{q}_v'' A \qquad \textbf{(28)}$$

Using the conservation of mass equation (23), this can be rewritten as

$$\frac{\dot{m}''}{(1-\phi)} \Delta H_v = \dot{q}_k'' - \dot{q}_v'' \qquad \textbf{(29)}$$

where ΔH_v is the heat of pyrolysis, defined to be the difference in enthalpy between the virgin material and the char and volatiles at the pyrolysis temperature, T_v.

$$\Delta H_v \equiv h_v(T_v) - h_c(T_v) + h_g(T_v) \tag{30}$$

The conducted heat fluxes $\dot{q}_k''$ and $\dot{q}_v''$ can be determined using the temperature profiles within the virgin material and char layer, respectively. Using these profiles (derived in the next two sections), equation 29 can be reduced to

$$\frac{\dot{m}''}{(1-\phi)}\Delta H_v = \left(-2k\frac{(T_v - T_0)}{\delta_v(t)}\right) - \left(-k_c\frac{(T_s(t) - T_v)}{\delta_c(t)}\right) \tag{31}$$

Virgin material

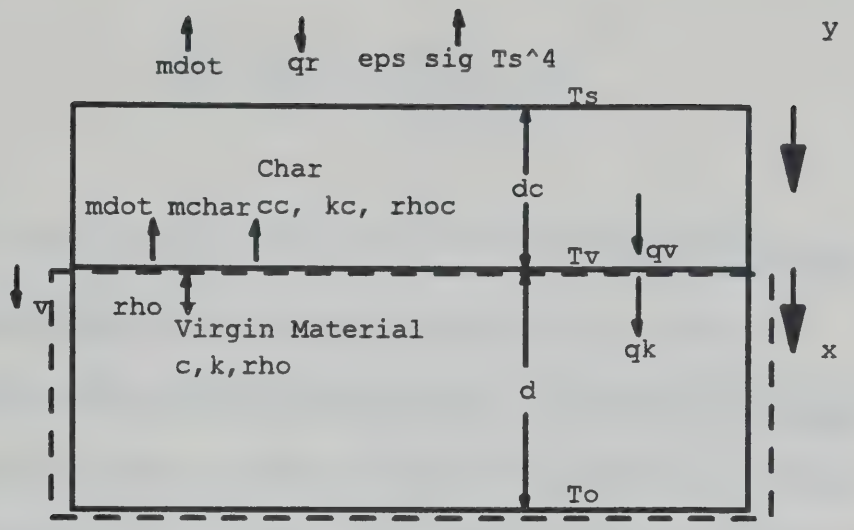

Figure 5 Control volume surrounding the virgin material

Conservation of mass

Consider a mass balance on the control volume surrounding the virgin material. This control volume is shown in figure 5. Mass enters the control volume from the substrate as the thermal layer grows, and mass exits the control volume as the vaporization plane advances into the material. In equation form, the conservation of mass is:

$$\frac{dm_v}{dt} = \rho \frac{d\delta_v}{dt} A - \rho v A \qquad (32)$$

This equation can be simplified to

$$\frac{1}{A}\frac{dm_v}{dt} = \rho\left(\frac{d\delta_v}{dt} - v\right) \tag{33}$$

Temperature Profile

In order to apply the integral method to the conservation of energy equation, a temperature profile must be determined. Examining the control volume surrounding the virgin material in figure 5, note the conditions on the virgin material. At the top surface x=0, bordering the vaporization plane, the temperature is fixed at T_v, and there is a heat flux q_k'' conducted into the virgin material. At the bottom surface $x=\delta_v(t)$, bordering the substrate, the temperature is constant at T_0 and there is no heat conducted into the substrate. From these four boundary conditions, only three (Constant temperature T_v and T_0, and an insulated bottom surface) will be used so that a quadratic temperature profile will be determined. The profile is assumed to have the form

$$T(x,t) = A(t) + B(t)x + C(t)x^2 \tag{34}$$

and to have the boundary conditions:

$$T(0,t) = T_v \qquad T(\delta_v(t),t) = T_0 \qquad -k\left.\frac{dT}{dx}\right|_{x=\delta_v(t)} = 0 \tag{35}$$

Using the analysis from Chapter Three, the temperature profile is found to be:

$$(T-T_0) = (T_v-T_0)\left(1-\frac{x}{\delta_v(t)}\right)^2 \qquad (36)$$

This temperature profile that will be used in the conservation of energy.

Conservation of Energy

Now consider an energy balance on the control volume enclosing the virgin material, shown in figure 5. Energy is gained by conduction into the material through the vaporization plane, $\dot{q}''_k$. Energy is lost from the control volume where mass is consumed by the vaporization plane, $\rho v A h_v(T_v)$. Using these relationships, the conservation of energy is expressed as

$$A\rho c\frac{d}{dt}\int_0^{\delta(t)}(T-T_0)dy = \dot{q}_k - A\rho vc(T_v-T_0) \qquad (37)$$

Applying the temperature profile (equation 36) and integrating yields:

$$\frac{\rho c}{3}\frac{d\delta_v}{dt}+\frac{\dot{m}''c}{(1-\phi)} = \frac{2k}{\delta_v(t)} \qquad (38)$$

Char

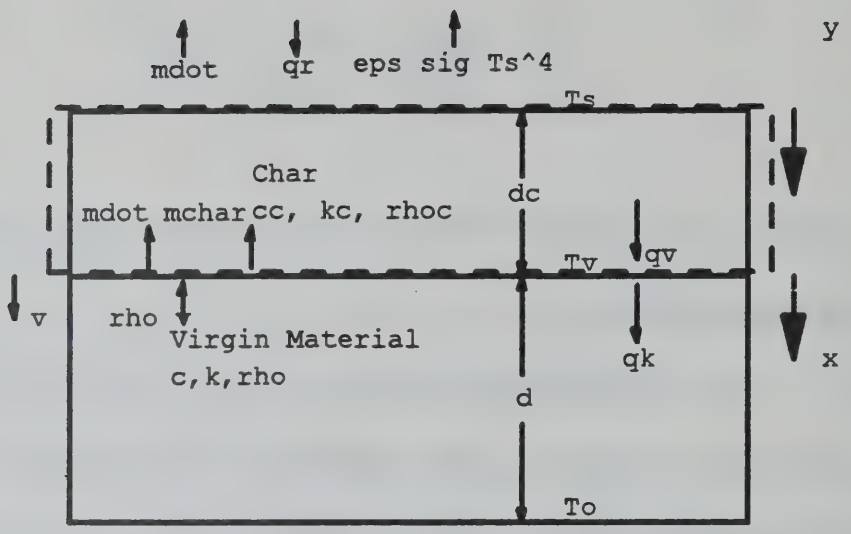

Figure 6 Control volume enclosing the char layer

Conservation of mass

The third region of the material is the char. It is this layer that separates this problem from the previously solved thermoplastic problem[11]. Consider a control volume enclosing the char, shown in figure 6. Mass enters the control volume through the bottom surface, at $y=\delta_c(t)$, where the vaporization plane deposits char and generates volatiles. Mass exits the control volume at the top surface, y=0, where the volatiles escape. Expressed mathematically:

$$\frac{dm_c}{dt} = A(\dot{m}''_{vp} + \dot{m}''_c) - A\dot{m}''_{surface} \qquad (39)$$

Since the volatiles are assumed to exit the char upon formation, $\dot{m}''_{vp} = \dot{m}''_{surface}$, and this can be rewritten:

$$\frac{1}{A}\frac{dm_c}{dt} = \dot{m}_c'' \tag{40}$$

Temperature Profile

Before developing the conservation of energy equation for the char, some temperature profile must be assumed. Consider the boundary conditions of the control volume. At $y=\delta_c(t)$, the temperature is constant at T_v, and the heat flux into the vaporization plane is $\dot{q}_v''$. At $y=0$, the temperature is $T_s(t)$ and the heat flux into the char is $\dot{q}_r''$. From these four boundary conditions, the temperature conditions will be used. Because the char layer is thin, it is unlikely that the temperature profile will deviate significantly from linear. For this reason, and in the interest of simplicity, there is no reason to develop a more complicated profile. Assuming a profile of the form:

$$T(x,t) = A(t) + B(t)x \tag{41}$$

and using the boundary conditions:

$$T(0,t) = T_s(t) \qquad T(\delta_c(t),t) = T_v \tag{42}$$

yields the profile:

$$T(y,t) - T_v = (T_s(t) - T_v)\left(1 - \frac{y}{\delta_c(t)}\right) \tag{43}$$

that can be substituted into the conservation of energy.

Conservation of energy

Now consider an energy balance on the control volume enclosing the char, shown in figure 6. Energy is gained by the control volume three ways: the incident radiation, $\dot{q}_r"A$; the enthalpy carried by the char deposited into the control volume, $\dot{m}_c"Ah_c(T_v)$; and the enthalpy carried by the volatile gas, $\dot{m}"Ah_g(T_v)$. Energy is lost from the control volume three ways: heat conducted into the vaporization plane, $\dot{q}_v"A$; and enthalpy carried by the volatiles, $\dot{m}"Ah_g(T_s)$; and the surface re-radiation, $\epsilon\sigma T_s^4$. Expressed mathematically:

$$\begin{aligned} &A\rho_c c_c \frac{d}{dt}\int_0^{\delta_c(t)} (T - T_0)dy = \\ &A\left(\dot{m}_c'' c_c (T_v - T_0) + \dot{m}'' c_g (T_v - T_0) + \dot{q}_r''\right) - A\left(\dot{q}_v'' + \dot{m}'' c_g (T_s(t) - T_0) + \epsilon\sigma T_s(t)^4\right) \end{aligned} \tag{44}$$

Simplifying the above equation, and using equation 43, this reduces to

$$\frac{\rho_c c_c}{2}\frac{d}{dt}\left[\delta_c(t)\left(T_s(t)+T_v-2T_0\right)\right]+\dot{m}''c_g(T_s(t)-T_v)-\dot{m}_c''c_c(T_v-T_0)= \dot{q}_r''-\epsilon\sigma T_s(t)^4-k_c\frac{(T_s(t)-T_v)}{\delta_c(t)} \quad (45)$$

Using the the product rule for differentiation and the relationship between $\dot{m}_c$" and $\dot{m}$" from equation 27, equation 45 can be further rewritten

$$\frac{\rho_c c_c}{2}\left[\frac{d\delta_c}{dt}\left(T_s(t)+T_v-2T_0\right)+\delta_c(t)\frac{dT_s}{dt}\right]+ \dot{m}''\left[c_g(T_s(t)-T_v)-\frac{\phi}{(1-\phi)}c_c(T_v-T_0)\right]=\dot{q}_r''-\epsilon\sigma T_s(t)^4-k_c\frac{(T_s(t)-T_v)}{\delta_c(t)} \quad (46)$$

Conclusions

The four equations constituting the model have been derived from the principles of conservation of mass and energy. They comprise a system of three ordinary differential equations and one algebraic equation, shown below:

$$\frac{d\delta_c}{dt}=\frac{\dot{m}''}{\rho(1-\phi)} \quad (26)$$

$$\frac{\dot{m}''}{(1-\phi)}\Delta H_v = \left(-2k\frac{(T_v - T_0)}{\delta_v(t)}\right) - \left(-k_c\frac{(T_s(t) - T_v)}{\delta_c(t)}\right) \tag{31}$$

$$\frac{\rho c}{3}\frac{d\delta_v}{dt} + \frac{\dot{m}''c}{(1-\phi)} = \frac{2k}{\delta_v(t)} \tag{38}$$

$$\begin{aligned}&\frac{\rho_c c_c}{2}\left[\frac{d\delta_c}{dt}\left(T_s(t) + T_v - 2T_0\right) + \delta_c(t)\frac{dT_s}{dt}\right] + \\ &\dot{m}''\left[c_g(T_s(t) - T_v) - \frac{\phi}{(1-\phi)}c_c(T_v - T_0)\right] = \dot{q}_r'' - \epsilon\sigma T_s(t)^4 - k_c\frac{(T_s(t) - T_v)}{\delta_c(t)}\end{aligned} \tag{46}$$

The dependant variables of interest are thermal penetration δ, char layer thickness δ_c, surface temperature T_s, and mass loss rate $\dot{m}''$.

This concludes the first phase of modelling -- formulating the problem. The next chapter begins the second phase of modelling, solving the equations.

Chapter 5 – Solving the Model

Introduction

The second stage of modelling is the solution of the governing equations. The first part of that solution process is nondimensionalizing the equations. Using dimensional analysis simplifies the problem and also draws attention to natural symmetries. The second part of the solution process is actually solving the equations. Solving the equations involves formulating the initial conditions, and in this case, using a series solution to escape the initial singularity followed by numerical solution using Mathematica™ software.

Dimensional Analysis

Rather than delve into a complete dimensional analysis, clues to appropriate dimensionless groups will be taken from previous work with non-charring materials, intuition, physics, and the organization of the terms in the equations.

Composite parameters

In the course of developing the dimensionless groups, three new dimensional parameters occur frequently. While these composite parameters arise in part out of convenience, they have very important physical meanings. The first parameter is the heat of gasification, L, which represents the energy required to pyrolyse material at the ambient temperature.

$$L = \Delta H_v + c(T_v - T_0) \qquad \textbf{(46)}$$

The second parameter, $\dot{q}_0''$, represents the net radiative flux at the surface at the time of ignition.

$$\dot{q}_0'' = \dot{q}_r'' - \epsilon\sigma T_v^4 \tag{47}$$

The third parameter, δ_s, arises from the modelling of non-charring pyrolysis and represents the depth of penetration of the thermal wave at steady state.

$$\delta_s = \frac{2kL}{c\dot{q}_0''} \tag{48}$$

This parameter forms a kind of characteristic length that will be referenced often in the dimensional analysis.

Dimensionless groups

The many dimensionless groups involved in a system of this complexity can be divided into three categories: independent variables, dependant variables, and problem parameters.

Independent Variables

The system under consideration consists of ordinary differential equations. There is therefore only one independent variable, time. The dimensionless time, τ, is a modified Fourier number:

$$\tau = \frac{4\alpha t}{\delta_s^2} \tag{49}$$

Dependant Variables

The system under consideration contains four equations, and there are accordingly four dependant variables. The objective of the model is to track the thermal layer penetration depth, δ; the thickness of the char layer, δ_c; the surface temperature, T_s; and the mass loss rate, $\dot{m}''$. The dimensionless thermal penetration and char layer are obtained by scaling to the characteristic length δ_s.

$$\Delta(\tau) = \frac{\delta(t)}{\delta_s} \quad \text{(a)} \qquad \Delta_c(\tau) = \frac{\delta_c(t)}{\delta_s} \quad \text{(b)} \tag{50}$$

The dimensionless temperature can be obtained by scaling to the vaporization temperature:

$$\theta_s(\tau) = \frac{T_s(t)}{T_v} \tag{51}$$

Finally, the dimensionless mass loss rate is obtained by scaling to the steady state mass loss rate for non-charring pyrolysis, given by $\dot{q}_0''/L$.

$$M(\tau) = \frac{\dot{m}''(t)L}{(1-\phi)\dot{q}_0''}$$

The additional factor $1/(1-\phi)$ adjusts for the char.

Problem Parameters

The system under consideration contains nine additional dimensionless parameters arising from either scenario inputs or material properties. The five most obvious parameters result from scaling the material properties by the virgin material properties. These are grouped below without further explanation.

$$\phi = \frac{\rho_c}{\rho}_{(a)} \qquad K = \frac{k_c}{k}_{(b)} \qquad \xi_c = \frac{c_c}{c}_{(c)} \qquad \xi_g = \frac{c_g}{c}_{(d)} \qquad \theta_0 = \frac{T_0}{T_v}_{(e)} \tag{53}$$

The remaining four parameters may be less obvious, and may require some further explanation.

$$\gamma = \frac{cT_v}{L}_{(a)} \qquad \lambda = \frac{cT_v}{\Delta H_v}_{(b)} \qquad \beta = \frac{L}{\Delta H_v} = \frac{\lambda}{\gamma}_{(c)} \qquad \eta = \frac{\dot{q}_0''}{\epsilon\sigma T_v^4}_{(d)} \tag{54}$$

λ represents the ratio of the sensible enthalpy of the material at the pyrolysis temperature to the latent enthalpy required to pyrolyse the material at the pyrolysis temperature. Similarly γ represents the ratio of the sensible enthalpy of the material at the pyrolysis temperature to the latent enthalpy required to pyrolyse the material from the ambient temperature. β is the ratio of the heat of gasification to the heat of pyrolysis. η represents the ratio of the net radiant heat flux on the surface to the

re-radiated heat flux. Note that, by the definition of L, λ and γ are not independent, but are related by the expression:

$$\lambda = \frac{1}{\gamma} - (1 - \theta_0) \tag{55}$$

Dimensionless form of the equations

These fourteen dimensionless groups enable the governing equation to be reduced to a slightly simpler system, presented below.

(*a*) From equation 46:

$$2\phi\xi_c\left[\frac{d\Delta_c}{d\tau}\left(\theta_s(\tau)+1-2\theta_0\right)+\Delta_c(\tau)\frac{d\theta_s}{d\tau}\right]+$$

$$2M(\tau)\left[\xi_g(1-\phi)\left(\theta_s(\tau)-1\right)-\phi\xi_c(1-\theta_0)\right]=\frac{2}{\gamma}\left(1-\frac{(\theta_s(\tau)^4-1)}{\eta}\right)-\frac{K\left(\theta_s(\tau)-1\right.}{\Delta_c(\tau)}$$

(*b*) From equation 31

$$\frac{2M(\tau)}{\lambda} = \frac{K\left(\theta_s(\tau)-1\right)}{\Delta_c(\tau)} - \frac{2(1-\theta_0)}{\Delta(\tau)} \tag{56}$$

(*c*) From equation 26

$$\frac{d\Delta_c}{d\tau} = \frac{M(\tau)}{2}$$

(*d*) From equation 38

$$\frac{2}{3}\frac{d\Delta}{d\tau} + M(\tau) = \frac{1}{\Delta(\tau)}$$

Solving the equations

Having completed a dimensional analysis on the system, attention can be turned to arriving at a solution. First the initial conditions will be presented in dimensionless

form, then a series solution will be developed to avoid the singularity in the initial conditions, and finally the solution method will be described.

Initial Conditions

In the formulation of the model, the initial conditions are qualitatively stated. The model equations are valid from the time pyrolysis commences, t_{ig}. At this time, the surface temperature, T_s, has just reached the vaporization temperature, T_v. No pyrolysis has occurred, so the char layer thickness, δ_c, is 0 and the mass loss rate, $\dot{m}''$, is also 0. The thermal penetration, δ, has a value δ_{ig} found from

$$\delta_{ig} = \sqrt{6\alpha t_{ig}} \tag{57}$$

This was derived in chapter 3. The time pyrolysis begins can be estimated by

$$t_{ig} = \frac{2}{3} k\rho c \left(\frac{T_{ig} - T_0}{\dot{q}_0''} \right)^2 \tag{58}$$

Equation 58 can be substituted into equation 57, and the dimensional analysis of the preceding section applied to find the dimensionless forms of the conditions suitable for use in the dimensionless system.

$$\Delta_{ig} = \gamma(1-\theta_0)_{(a)} \qquad \tau_{ig} = \frac{2}{3}\gamma^2(1-\theta_0)^2 = \frac{2}{3}\Delta_{ig}^2{}_{(b)} \tag{59}$$

The dimensionless initial conditions are presented below:

$$\Delta_{ig} = \gamma(1-\theta_0)_{(a)} \quad \Delta_{c,ig} = 0_{(b)} \quad \theta_{s,ig} = 1_{(c)} \quad M_{ig} = 0_{(d)} \tag{60}$$

Series Solution

An examination of the system at the initial conditions finds a disturbing complication. The singular term

$$\frac{\theta_{s,ig}-1}{\Delta_{c,ig}} = \frac{0}{0} \tag{61}$$

appears in equations 56(a) and (b). To avoid this singularity, adjusted initial conditions are obtained from a series solution. A series of the form

$$p(\tau) = p_{ig} + \tilde{p}\tau \tag{62}$$

is assumed valid for $\tau << 1$for each dependant variable is substituted into the system. Neglecting terms $O(\tau^2)$, the equations reduce to a linear system:

(a)

$$2\phi\xi_c\left[\tilde{\Delta}_s(\theta_{s,ig}+\tilde{\theta}_s\tau+1-2\theta_0)+(\Delta_{c,ig}+\tilde{\Delta}_c\tau)\tilde{\theta}_s\right]+$$
$$2(M_{ig}+\tilde{M}\tau)\left[\xi_g(1-\phi)\left(\theta_{s,ig}+\tilde{\theta}_s\tau-1\right)-\phi\xi_c(1-\theta_0)\right]=$$
$$\frac{2}{\gamma}\left(1-\frac{(\theta_{s,ig}^4+4\theta_{s,ig}^3\tilde{\theta}_s\tau-1)}{\eta}\right)-\frac{K(\theta_{s,ig}+\tilde{\theta}_s\tau-1)}{\Delta_{c,ig}+\tilde{\Delta}_c\tau}$$

(b)

$$\frac{2M_{ig}+\tilde{M}\tau}{\lambda}=\frac{K(\theta_{s,ig}+\tilde{\theta}_s\tau-1)}{\Delta_{c,ig}+\tilde{\Delta}_c\tau}-\frac{2(1-\theta_0)}{\Delta_{ig}+\tilde{\Delta}\tau} \qquad (63)$$

(c)

$$\frac{d\Delta_c}{d\tau}=\frac{M_{ig}+\tilde{M}\tau}{2}$$

(d)

$$\frac{2}{3}\tilde{\Delta}+M_{ig}+\tilde{M}\tau=\frac{1}{\Delta_{ig}+\tilde{\Delta}\tau}$$

Since the initial conditions are known, this can be solved for the $\tilde{p}$ terms assuming a small time increment τ^*. The adjusted initial conditions are then given by

$$\Delta^*(\tau)=\Delta_{ig}+\tilde{\Delta}\tau^* \quad \text{(a)} \qquad \Delta_c^*(\tau)=\tilde{\Delta}_c\tau^* \quad \text{(b)}$$
$$\theta_s^*(\tau)=1+\tilde{\theta}_s\tau^* \quad \text{(c)} \qquad M^*(\tau)=\tilde{M}\tau^* \quad \text{(d)} \qquad (64)$$

Solution method

With the initial conditions adjusted to avoid the singularity, attention can be turned to producing a solution for the model. The nonlinear nature of the equation makes it prohibitively difficult to develop a closed form analytical solution, and the

coupling of the differential equations with the algebraic equation makes it difficult to use canned numerical methods on the whole system. One solution to this dilemma would be to write a numerical scheme such as Runge-Kutta to the differential equations and another scheme such as Newton-Raphson to solve the algebraic equation for each time step of the Runge-Kutta routine. While Runge-Kutta is a dependable scheme, for best results an adaptive time-step algorithm should be used, and implementing the adaptive time-step increases the complexity of the program. An alternative would be to explicitly solve one equation for one dependant variable, and then substitute this solution into the other three equations This produces a system of three coupled, nonlinear differential equations that is amenable to canned numerical routines. Once the solution has been obtained, the values for each time step can be back-substituted into the remaining equation, and the complete solution thus obtained.

In the current work the second approach is used. Solving equation 56c for M yields:

$$M(\tau) = 2\frac{d\Delta_c}{d\tau} \tag{65}$$

This can be substituted into the remaining three equations to find:

(*a*)

$$2\phi\xi_c\left[\frac{d\Delta_c}{d\tau}\left(\theta_s(\tau)+1-2\theta_0\right)+\Delta_c(\tau)\frac{d\theta_s}{d\tau}\right]+$$
$$4\frac{d\Delta_c}{d\tau}\left[\xi_g(1-\phi)\left(\theta_s(\tau)-1\right)-\phi\xi_c(1-\theta_0)\right]=\frac{2}{\gamma}\left(1-\frac{(\theta_s(\tau)^4-1)}{\eta}\right)-\frac{K\left(\theta_s(\tau)-1\right.}{\Delta_c(\tau)}$$

(*b*) **(66)**

$$\frac{4}{\lambda}\frac{d\Delta_c}{d\tau}=\frac{K\left(\theta_s(\tau)-1\right)}{\Delta_c(\tau)}-\frac{2(1-\theta_0)}{\Delta(\tau)}$$

(*c*)

$$\frac{2}{3}\frac{d\Delta}{d\tau}+2\frac{d\Delta_c}{d\tau}=\frac{1}{\Delta(\tau)}$$

Using Mathematica™ software, the series solution and substitutions can be collected into a single routine. The function CharSolve was developed to take a sequence of material property values and return functions for the thermal penetration, char thickness, surface temperature and mass loss rate. Functions were also written to prepare labeled plots of the functions and to discretize the functions and return lists of data more suitable for further manipulation. These functions are included in their entirety in Appendix I

Conclusion

In this chapter the equations developed in Chapter Four were solved. The relevant dimensionless parameters to effect the solutions were derived. The equations were

solved by substituting one equation into the other three. The system can be solved and the fourth quantity is found from the back substitution.

Chapter 6 -- Model results

Introduction

The third stage of modelling is comparison of the solution to known data. After all, the purpose of modelling is to try to gain some insight into what factors and phenomena are relevant to a physical process. A model that cannot show reasonable agreement with data cannot be used to arrive at this insight.

In this chapter, results from the model are presented. They will first be compared with Delichatsios and deRis[5]. Next they will be compared with Chen[2]. Then, they will be compared with some experimental data presented by Kashiwagi, Ohlemiller, and Werner[14]

Delichatsios and deRis

Delichatsios and deRis[5] developed a model for the pyrolysis of charring materials. Their model holds for the later stages of pyrolysis, after the mass loss has peaked and is declining. Like the present model, they used the integral approximation to solve the transient heat transfer process and assumed constant temperature pyrolysis with a constant heat requirement. Unlike the present model, they used exponential profiles in the char and virgin material and developed the governing equations using a temperature moment method. Also, they assumed a variable thermal conductivity within the material based on a radiative-interstitial heat transfer model, with $k_c \propto T^3$. Their selection of k_c confers two main advantages: it models the increase in

conductivity with temperature, and more important, it provides a closed form pyrolysis rate expression.

Their work has the advantage of resulting in a closed form solution for the mass loss rate. They develop two expressions for mass loss, one general equation and one simpler for long times. Figure 7 shows their two equations plotted with the results from the current work.

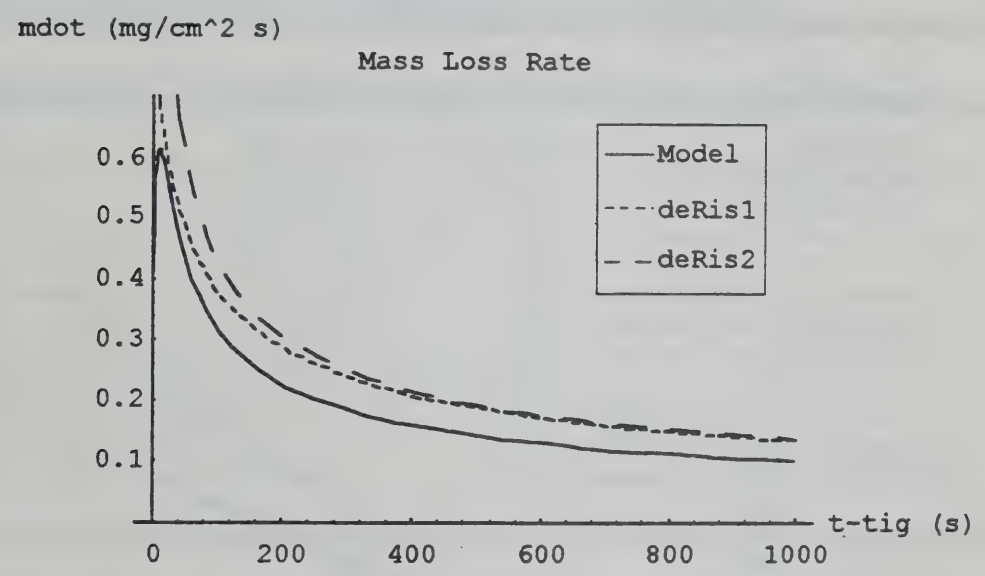

Figure 7 Comparison against Delichatsios and de Ris

In this figure, the origin has been shifted to the time of ignition. The line marked deRis 1 represents the more general equation, while deRis 2 represents the longer time expression. For small time, the general equation seems to track well with the current model, while the long time equation predicts a higher pyrolysis rate. For long time, the current model under-predicts the mass loss rate, compared with both equations. This is

not particularly surprising, since the Delichatsios and deRis model involves a higher thermal conductivity in the char, permitting more heat conduction and thus providing more heat to the pyrolysis process. The current model also includes the energy stored in the char layer, something neglected in the Delichatsios and deRis model. This energy storage further reduces the energy available for pyrolysis, thus further reducing the pyrolysis rate. It is important to note, however, that despite the under-prediction the current model and the Delichatsios and deRis model do show approximately the same character for the mass loss expression, $\dot{m}''$ varying with $t^{-\frac{1}{2}}$. This relationship is more clear in figure 8

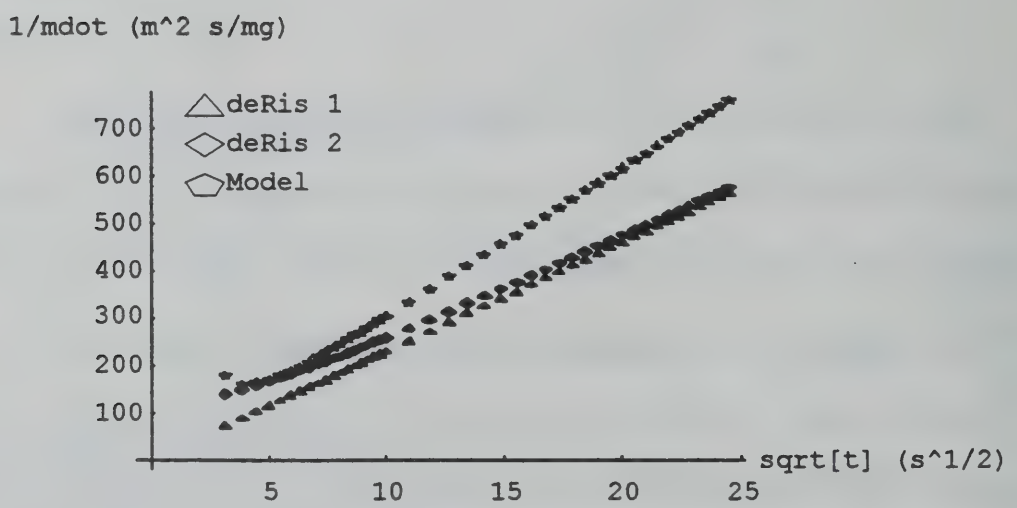

Figure 8 Re-scaled plot of deRis vs. the current model

Figure 8 shows two aspects of the models. First, that $\dot{m}''$ is proportional to $t^{-1/2}$. It also more clearly shows that the current model decays more quickly that the Delichatsios and deRis model.

The material properties used in the Delichatsios and deRis comparisons are given in table 1. These are the defaults for the CharSolve routine, and were selected as typical values suggested by the literature.

Table 1 Properties for Delichatsios and de Ris comparisons

Property	Value	Property	Value
$\dot{q}_0''$	50 kW/m^2	L	3000 kJ/kg
c	1 kJ/kg K	c_c	1 kJ/kg K
ρ	700 kg/m^3	ϕ	.05
k	.08 W/m K	k_c	.05 W/m K
T_0	300 K	T_v	700 K
ϵ	.9	c_g	1.04 kJ/kg K

Chen

Chen's model [2] follows that of Delichatsios and deRis quite closely. Like Delichatsios and deRis, he uses the approximate integral method to solve the transient heat conduction and develops the equations using a temperature moment method. He extends their derivation to include the earlier development of the char layer, and he is able to get analytical solutions by assuming various incident heat flux histories.

The current model will be compared with his results for a constant imposed heat flux. Figure 9 shows this comparison.

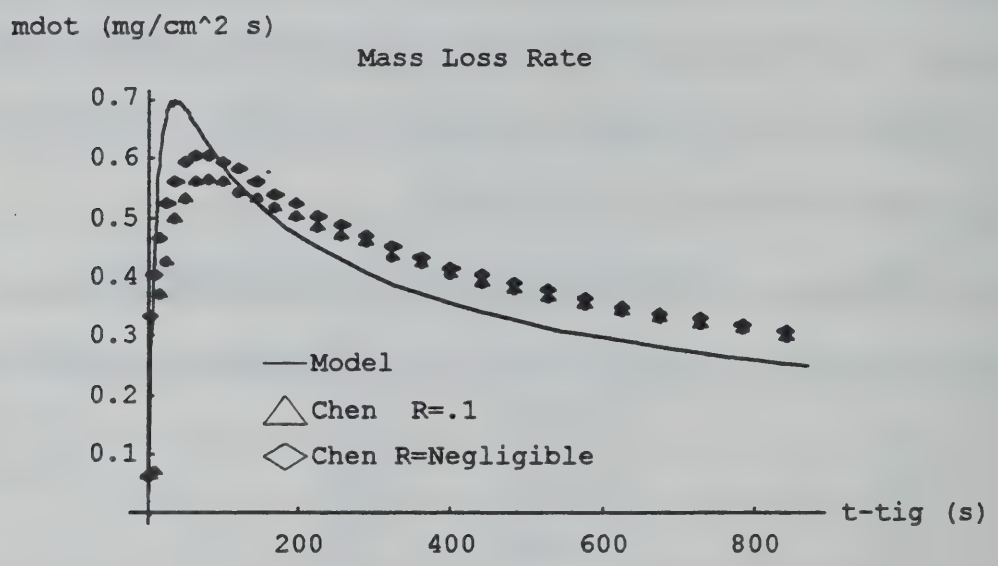

Figure 9 Comparison of mass loss rates (Chen and current)

As this shows, the current model predicts an earlier, taller peak than Chen's model. Figure 10 shows the same graphs with a shorter time scale to focus on the peak.

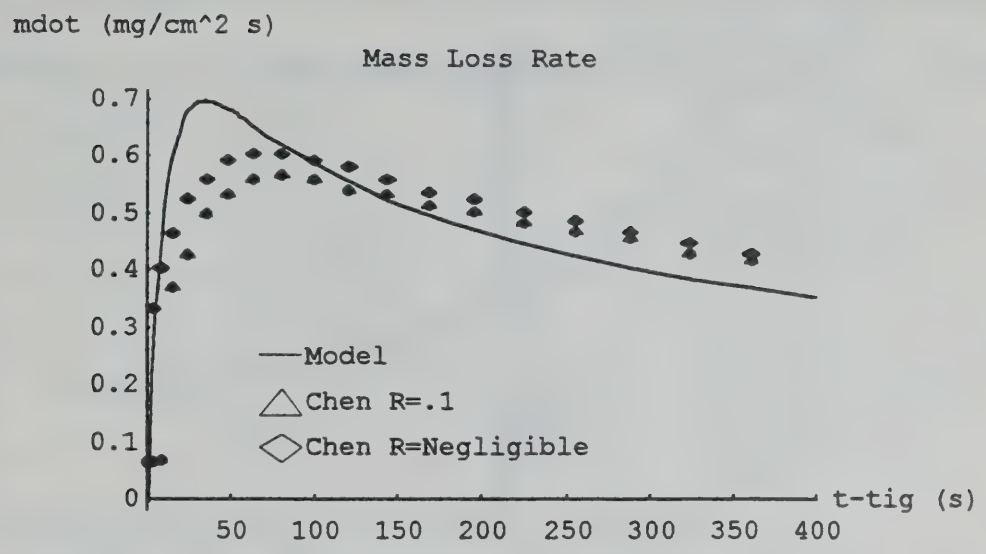

Figure 10 Plot focussing on the peak behavior (Chen and current)

In figures 9 and 10, Chen used a variable thermal conductivity identical to Delichatsios and deRis. Comparing the results again indicates that the variable conductivity model predicts a higher mass loss rate in the tail, probably resulting from increased conduction through the char layer. Figure 11 shows a comparison between the current model and Chen's for constant char thermal conductivity.

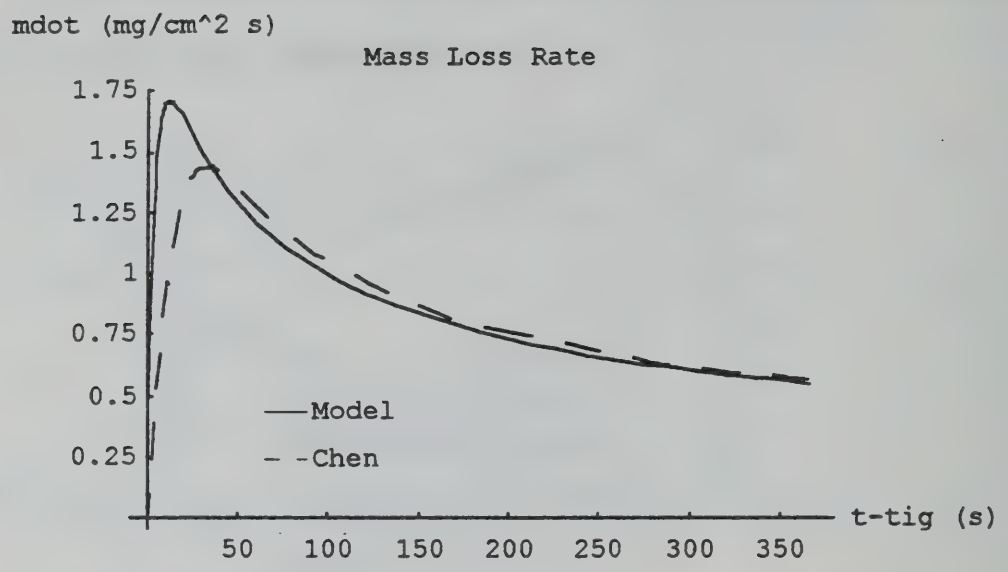

Figure 11 Comparison to Chen for constant thermal conductivity.

The current model shows good agreement with Chen's. Again, the peak occurs slightly before and is somewhat taller than Chen's, but the two tails agree extremely well. .

One advantage to making comparisons with other models is that the properties are often readily available. The properties used in these comparisons are listed in table 2.

Table 2 Properties used in the Chen Comparisons

Property	Value	Property	Value
$\dot{q}_0$" (figures 9,10)	20 kW/m^2	ΔH_v	76250 J/kg
$\dot{q}_0$" (figure 11)	30 kW/m^2	c_c	*1500 kJ/kg K*
c	1500 J/kg K	c_g	0 kJ/kg K
ρ	1200 kg/m^3	ϕ	*.10*
k	.2403 W/m K	k_c	.2403 W/m K
T_0	*300 K*	T_v	640 K
ϵ	*.9*		

The four properties in italics are those not explicitly specified by Chen. The first two, ϕ and c_c, were implicitly determined from Chen's properties. Chen uses a parameter R that is the ratio of the thermal capacity of the char to that of the virgin material. For the current model the components of thermal capacity (density and specific heat) are needed individually, so the specific heat of char was assumed equal to the virgin material. In this case, ϕ equals R. Finally, since Chen did not explicitly specify T_0 and ϵ, they were simply assumed to be typical values.

Ohlemiller, Kashiwagi, and Werner

Comparisons to other models are useful, but a model must compare well to experiment to be considered valid. Ohlemiller, Kashiwagi, and Werner [14] performed experiments investigating the pollutant species generated by wood burning stoves, and

some of their results can be compared with the predictions of the current model. In these experiments, they exposed small wooden blocks, approximately 3.8 cm cubes, to a range of heat fluxes in a variety of atmospheres and recorded the mass loss.

Comparisons to experimental data require particular caution. The experiments may have been conducted in a way that includes phenomena neglected in the model, and these additional effects must be acknowledged. For example, figure 12 shows two of Ohlemiller's experimental runs.

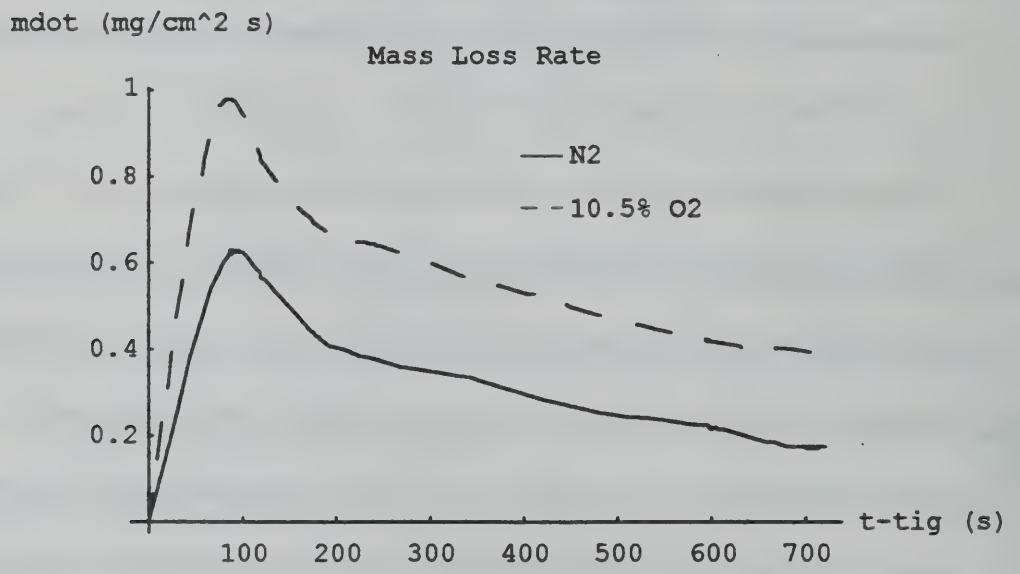

Figure 12 Comparison of mass loss in inert and oxygenated atmospheres

Both runs were conducted at 40 kW/m² using identical white pine samples. The difference between the two is that the dashed line represents the mass loss in an atmosphere of 10% O_2 in N_2, while the solid line represents the mass loss in an atmosphere of pure N_2. The oxygenated atmosphere shows a mass loss rate 50%

greater than the inert atmosphere throughout the experiment, probably resulting from secondary reaction effects. The current model does not include such effects.

The other primary difficulty in comparing to experimental data involves selecting appropriate physical properties. There is little difficulty matching properties in comparisons between models, so differences between outcomes can confidently be attributed to differences within the assumptions or solution methods. Experimental results may not report the full set of input parameters required by the model, and this complicates attempts to draw comparisons. The model must be run for various combinations of reasonable properties and comparisons drawn from the aggregate set.

Ohlemiller, Kashiwagi, and Werner reported only a few properties in their results. Additional properties were primarily determined from data in Janssens[13] and Suuberg[19]. The baseline property data used in the following comparisons are summarized in table 3.

Table 3 Property values used in Ohlemiller Comparisons

Property	Value	Source	Property	Value	Source
k	.095 W/m K	[13]	k_c	.016 W/m K	[19]
ρ	360 kg/m^3	[14]	ϕ	.25	[14]
c	2600 J/kg K	[13]	c_c	3200 J/kg K	[19]
L	2 MJ/kg	[13]	T_v	580 K	[13]
$\dot{q}_i''$	25,40,70 kW/m^2	[14]	ϵ	.5	[19]

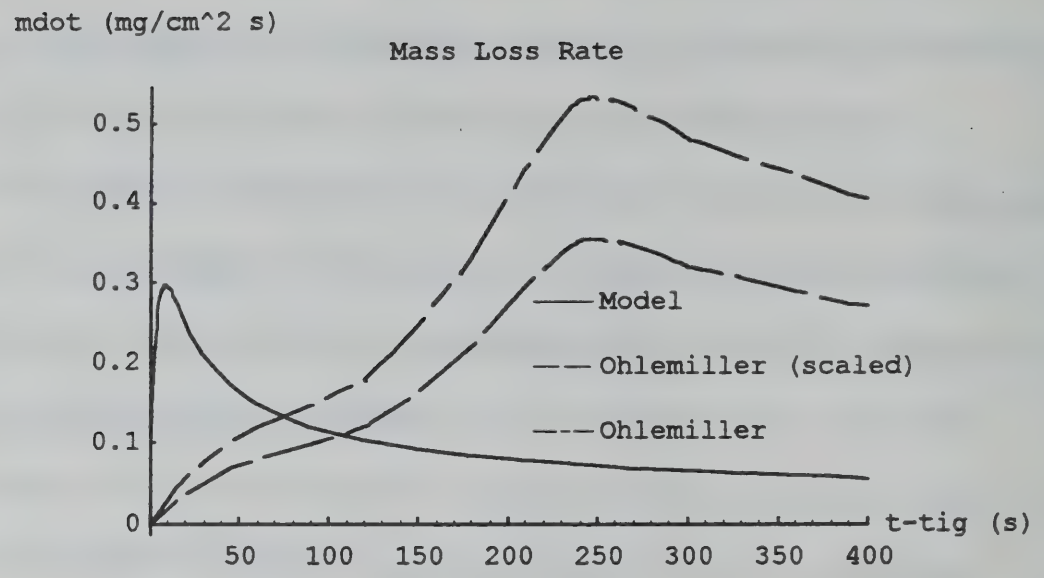

Figure 13 Base case for 25 kW/m^2 vs. Ohlemiller

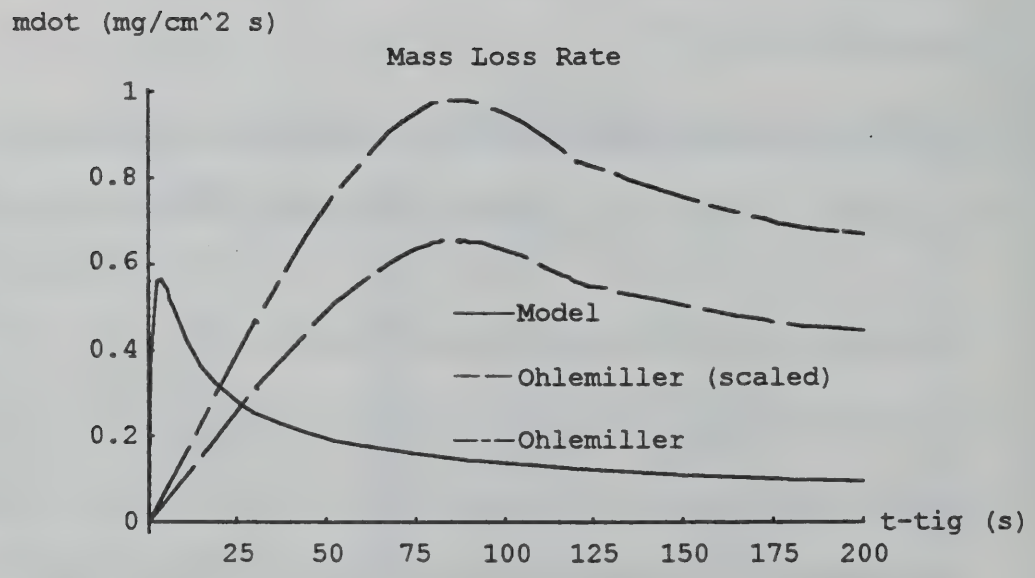

Figure 14 Base case for 40 kW/m^2 vs. Ohlemiller

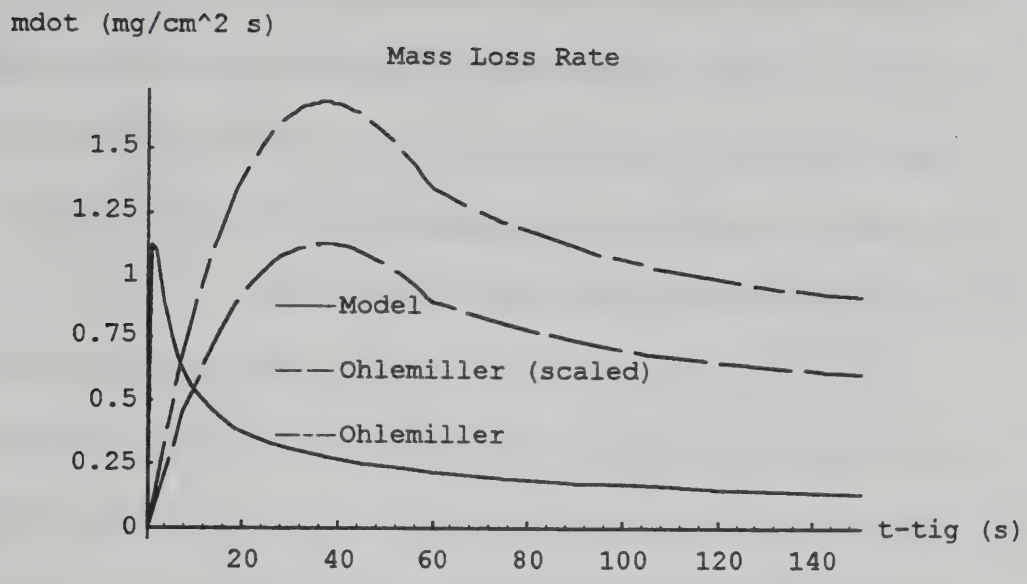

Figure 15 Base case for 70 kW/m^2 vs. Ohlemiller

Figures 13, 14, and 15 show the model predictions using the base case data from table 3 against the results presented by Ohlemiller for each heat flux imposed. Unfortunately, these data are only presented for the 10% O_2 atmosphere, which results in a 50% increase in mass loss rate (see figure 12). To compensate, the increase is assumed to be a constant proportion over all three heat fluxes, and the Ohlemiller data is multiplied by ⅔ to counteract the increase. After the data is scaled, the magnitude of the predicted mass loss peaks seems to match the experiments for all three cases. The timing of the peaks shows poor agreement in all three cases. This is not readily explicable. It may reflect a difference in the nature of the initial mass lost. The samples used in the experiments had been conditioned at 50% humidity, so the initial mass loss

is dominated by the water vapor for approximately the first 20-30 seconds. Also note that there is a marked disparity between the predicted tails and the experimental tails. Again, no explanation is readily apparent. This probably does not stem from the size of the samples. The samples were approximately 4 cm thick, so using equation 9, 10 the thermal wave takes over 2000s to reach the back surface.

To investigate the effect of the assumed properties on the mass loss rate, the heat of gasification, surface emissivity, and pyrolysis temperature are varied for the 40 kW/m^2 case. This permits the most direct comparison to experiment since it is the flux used in the inert atmosphere. Figures 16, 17, and 18 show these comparisons.

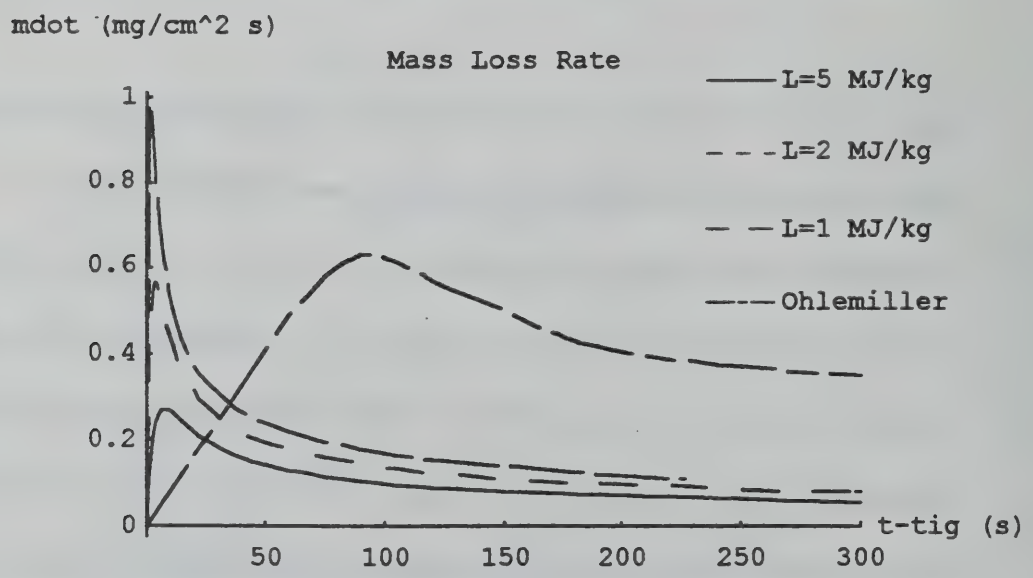

Figure 16 Effects of varying L for 40 kW/m^2

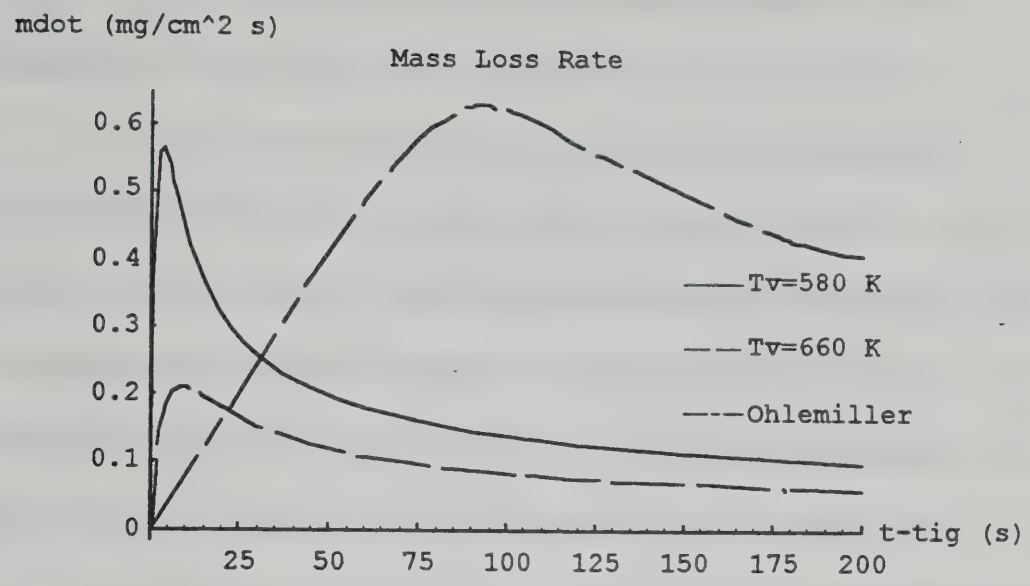

Figure 17 Effect of varying T_v for 40 kW/m^2

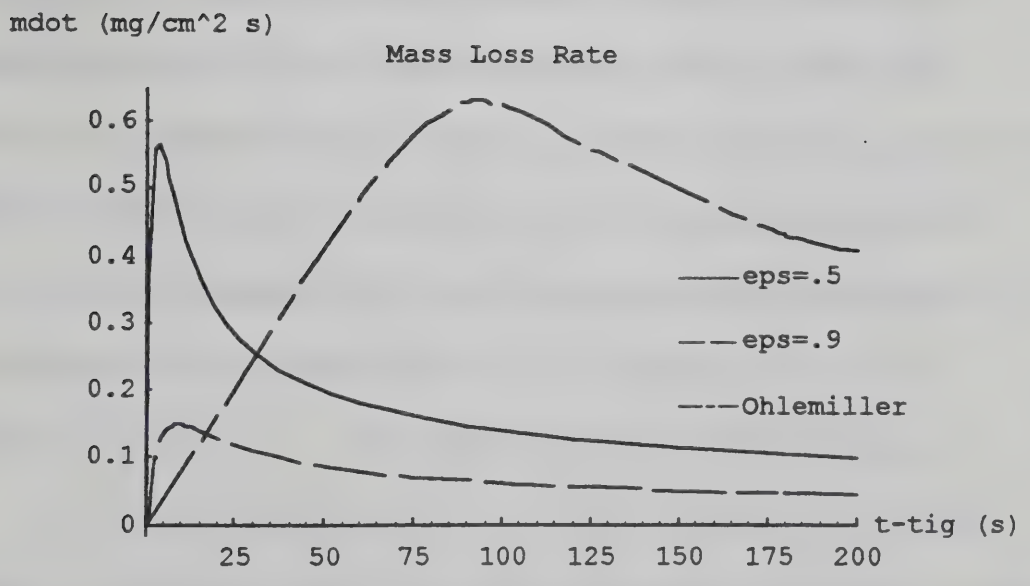

Figure 18 Effect of varying ϵ for the 40 kW/m^2 case

None of these changes has a particularly significant effect on the agreement between the model and experiment for the time of the peak or for the tails. They all have a fairly significant effect on the magnitude of the peak however.

It is interesting to note that the comparison with Chen's model (figure 10) shows better agreement with Ohlemiller's data. Despite a lower heat flux, the mass loss tail stays much higher than in the comparisons with Ohlemiller's data. Then again, Chen's heat of gasification was considerably less than suggested by literature values for wood. This underscores the importance of having accurate property data for materials.

Conclusions

The current model shows mixed results. It compares well to other models, even for non-constant properties. The agreement with experiment shows poorer agreement. The magnitude of the peak mass loss rate agrees well for pyrolysis in an inert atmosphere, but it is approximately ⅔ of the experimental value for an atmosphere of only 10% oxygen, perhaps because of secondary reaction effects. The time the peak occurs is wildly underpredicted by the current model, as is the long time mass loss rate. Comparisons of the experimental data against the model using the property values from Chen show much better agreement, and indicate the need for a method of determining the heat of gasification.

Chapter 7 – Applications of the model

Introduction

One of the aims of modelling is to gain understanding of a process. As discussed in the previous chapter, suitable property values must be used to a model for the model to accurately predict behavior. While it is possible for the failure of a model to be inappropriately attributed to faulty properties, many models suffer from a dearth of available data. One key property about which there is much conjecture is the heat of gasification. In this section, a method is proposed to obtain this property.

This idea behind this approach is that the pyrolysis process has two significant regimes. At the onset of pyrolysis, the material behaves similarly to a non-charring material. As the reaction proceeds, the effect of the char begins to dominate. If the mass loss peak occurs at the point these two sets of effects are equal, it would be possible to derive from this information the effective heat of gasification. This methodology simplifies the governing equations by making assumptions pertinent to the small time effects and then to the large time effects. In each case a solution for the mass loss rate is determined. These solutions are then equated, and the target data can be obtained.

Small time ($\tau \approx \tau_{ig}$)

For the short time approximation, the material is treated as a non-charring material. For this case, the surface temperature is constant at the pyrolysis temperature and no char layer forms.

$$T_s(t) = T_v \quad \text{(a)} \qquad \delta_c(t) = 0 \quad \text{(b)} \tag{67}$$

In nondimensional form

$$\theta_s(\tau) = 1 \quad \text{(a)} \qquad \Delta_c(\tau) = 0 \quad \text{(b)} \tag{68}$$

Given these conditions only equations 56b and d convey meaningful information. Substitution of equations 68a and b into equation 56b presents an apparent singularity. This can be resolved by assuming the singular term, physically, is the incident radiant heat flux in the dimensional equations. Making the substitution, the equations become:

$$\frac{\dot{m}''}{(1-\phi)}\Delta H_v = \dot{q}_0'' - k\frac{(T_v - T_0)}{\delta_v} \tag{69}$$

$$\frac{\rho c}{3}\frac{d\delta_v}{dt} + \frac{\dot{m}'' c}{(1-\phi)} = \frac{2k}{\delta_v} \tag{70}$$

Which, after dimensional analysis, become:

$$\frac{2M(\tau)}{\lambda} = \frac{2}{\gamma} - \frac{2(1-\theta_0)}{\Delta} \tag{71}$$

$$\frac{d\Delta}{d\tau} + M(\tau) = \frac{1}{\Delta} \tag{72}$$

Solving equation 72 for M and substituting into equation 71

$$\frac{2}{3}\frac{d\Delta}{d\tau} = \frac{1}{\Delta} + \frac{\lambda(1-\theta_0)}{\Delta} - \beta = \beta\frac{1-\Delta}{\Delta} \tag{74}$$

This ordinary differential equation can be solved with the initial condition

$$\Delta(\tau_{ig}) = \Delta_{ig} = \gamma(1-\theta_0) \tag{75}$$

giving

$$\frac{1-\Delta}{1-\Delta_{ig}} = \exp\left(-(\Delta-\Delta_{ig}) - \frac{3}{2}\beta(\tau-\tau_{ig})\right) \tag{76}$$

the right-hand side of equation 76 can be approximated by a one-term Taylor expansion for $\Delta \approx \Delta_{ig}$ and $\tau \approx \tau_{ig}$ to give an approximate expression for Δ

$$\Delta \approx \Delta_{ig} + \frac{3}{2}\beta(\tau - \tau_{ig})\left(\frac{1-\Delta_{ig}}{\Delta_{ig}}\right) \tag{77}$$

Finally, equation 71 can be solved for M (and equation 77 substituted in)

$$M = \beta + \frac{\lambda(1-\theta_0)}{\Delta} = \beta + \frac{\lambda(1-\theta_0)}{\Delta_{ig} + \frac{3}{2}\beta(\tau - \tau_{ig})\left(\frac{1-\Delta_{ig}}{\Delta_{ig}}\right)} \tag{78}$$

Long Time ($\tau >> \tau_{ig}$)

In the long time approximation, the process has almost reached the steady state. In this case, Δ is considered large. Combining equations 56b and c for these conditions:

$$\frac{d\Delta_c}{d\tau} = \frac{1}{2}\left[\frac{\lambda}{2}\frac{K(\theta_s - 1)}{\Delta_c}\right] \tag{79}$$

This ordinary differential equation can be solved using the initial condition

$$\Delta_c(\tau_{ig}) = 0 \tag{80}$$

to find an expression for Δ_c

$$\Delta_c = \sqrt{\frac{\lambda K(\theta_s - 1)}{2}(\tau - \tau_{ig})} \tag{81}$$

Additionally, in this case the surface temperature has reached an equilibrium where re-radiation nearly equals the incident flux.

$$\dot{q}_r'' = \epsilon\sigma T_s^4 \quad \rightarrow \quad T_s = \frac{\dot{q}_r''}{\epsilon\sigma} \tag{82}$$

This can be expressed nondimensionally as:

$$\theta_s = \sqrt[4]{\eta + 1} \tag{83}$$

Finally, solving equation 56b (with the assumption that Δ is large) for M and substituting equations 81 and 83

$$M = \frac{\lambda K(\theta_s - 1)}{\Delta_c} = \frac{\lambda K(\sqrt[4]{\eta + 1} - 1)}{\sqrt{\frac{\lambda K(\sqrt[4]{\eta + 1} - 1)}{2}(\tau - \tau_{ig})}} \tag{84}$$

Implementing the approach

The basis of this approach is the idea that the mass loss peak occurs where these two approximations shift dominance, ie where they are equal. Assuming this occurs at τ_{peak}, τ_{peak} can be found by equating the two expressions for M.

$$M_{peak} = \frac{\lambda K(\sqrt[4]{\eta+1}-1)}{\sqrt{\frac{\lambda K(\sqrt[4]{\eta+1}-1)}{2}(\tau_{peak}-\tau_{ig})}} = \beta + \frac{\lambda(1-\theta_0)}{\Delta_{ig}+\frac{3}{2}\beta(\tau_{peak}-\tau_{ig})\left(\frac{1-\Delta_{ig}}{\Delta_{ig}}\right)} \quad (85)$$

Alternatively, one could obtain the peak mass loss and the time at which it occurs from experimental data, and choose the parameters of either equation (78 or 84) to match.

Figure 19, demonstrates this approach.

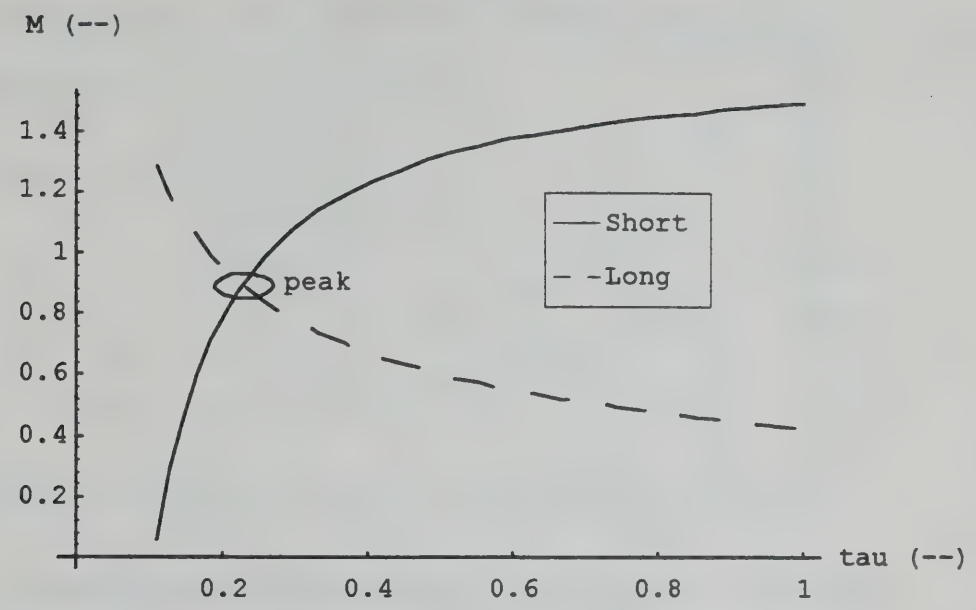

Figure 19 Comparing the short and long time approximations

The solid line represents the short time development, while the dashed line represents the long time mass loss behavior. The idea behind this approach is that the peak mass loss will occur at the intersection of the lines. As fig 19 demonstrates, the peak predicted by the model is quite different.

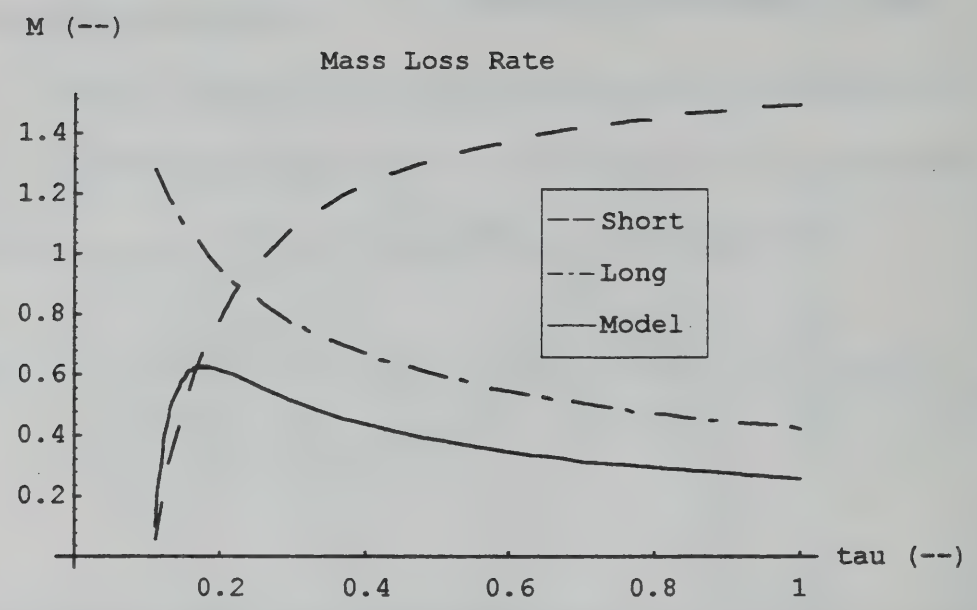

Figure 20 Compare approximations against model predictions

Figure 20 indicates that this approach is not quite successful. The mass loss peak occurs quite a bit before the prediction and also quite a bit below. This may be because the long time approximation overestimates the surface temperature. Equation 84 was developed by assuming θ_s had reaches a stationary value, and shows that M varies in proportion to $\sqrt{(\theta_s-1)}$. At the peak, θ_s may be as little as ¾ of the stationary value, and so the predicted peak may be off by as much as 50%. A correction factor, Ω, can be introduced such that

$$M_{revised} = \Omega\, M_{predicted} = \Omega \frac{\lambda K(\sqrt[4]{\eta+1}-1)}{\sqrt{\frac{\lambda K(\sqrt[4]{\eta+1}-1)}{2}(\tau-\tau_{ig})}} \qquad (86)$$

The correction factor corrects the mass loss rate for the surface temperature less than its maximum value. A careful selection of Ω can shift the long time curve to match the model mass loss rate, as shown in figure 21.

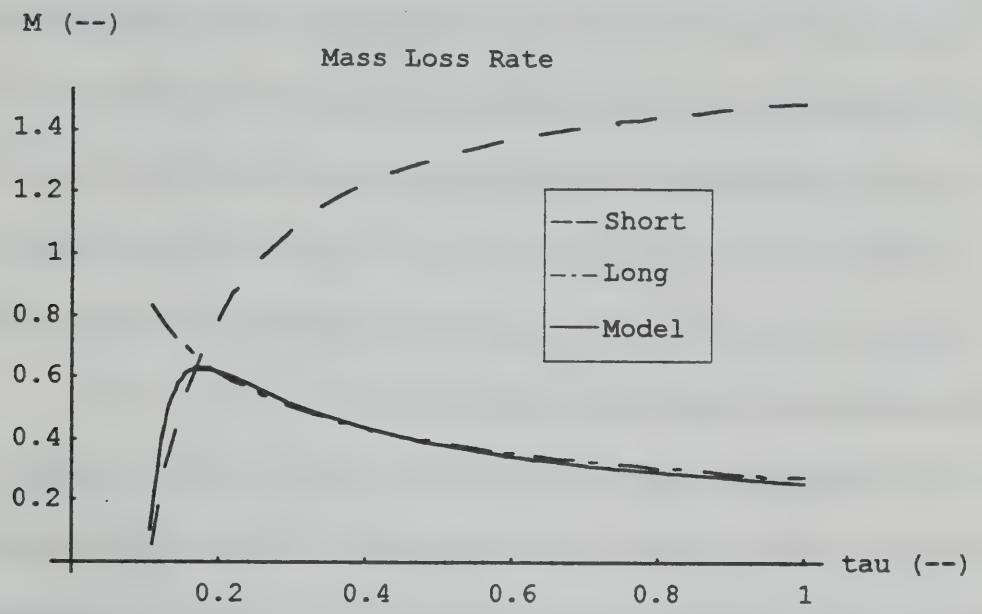

Figure 21 Comparing the corrected long time approximation to the predicted peak

For these plots the properties used in this plot are given in table 4.

Table 4 Properties used in the demonstration of the application

Property	Value	Property	Value
γ	.7	ξ_{sc}	1
λ	1.17	ξ_g	.5
η	4	K	.625
ϕ	.2	θ_0	.43
Ω	.65		

Conclusion

In this chapter a method for deriving the heat of gasification was developed using the current model. By solving the governing equations approximately for the long and short time behavior, the mass loss peak value and the time at which it occurs can be determined. Because the assumption of a stationary surface temperature (used in the long time solution) is not really valid, a correction factor was introduced, and the approximate solution yields good agreement when used with an appropriately chosen correction factor. If the surface temperature at peak mass loss is known, it can be used in the equations in place of the stationary value.

This approach might be used to derive the heat of gasification from experimental data. An iterative procedure of choosing a heat of gasification and comparing the experimental data with the approximate solution, then refining the guess until there is good agreement. This is not demonstrated as part of this work, merely presented.

Chapter 8 – Conclusions

The current work has developed a model for charring pyrolysis. The pyrolysis process is modelled for the following physical assumptions:

- Constant incident radiant flux
- Negligible convection at the surface
- Isothermal pyrolysis
- Constant material properties
- Semi-infinite material

This model divides the material into three regions; char, vaporization plane, and virgin material. The equations of conservation of mass and energy are formulated for each region. Transient heat transfer processes are modelled using the approximate integral method assuming polynomial temperature distributions. The resulting four equations are solved for the behavior of the thermal penetration, the char thickness, the surface temperature, and the mass loss rate. The equations contain a singularity at the onset of pyrolysis; this singularity is addressed by assuming one term series solutions for each of the four variables and thus "stepping away" from the initial singularity. The equations were solved using a Mathematica™ program.

The results from the model were compared with two other models and to some experimental data. The results compare well to the other models, while they compare poorly to the experimental data. This probably results from the difficulty in selecting values of material properties. In comparing to other models, all property values are

available. For experimental data, a full set of property values cannot, in general, be found.

A method has been suggested by which an effective heat of gasification can be deduced from experimental data. In this method, small time and large time approximations to the governing equation are made. By equating these two approximations (with an appropriate correction to the large time approximation) the time or magnitude of the mass loss peak can be predicted. The heat of gasification can then be chosen such that the prediction matches the experimental data.

Appendix I -- Mathematica Routine

```
Off[General::spell1,General::spell]

normL=L==dHv+c(Tv-To); (*heat of gasification*)
normqo=qo==qi-eps sig Tv^4;(*surface heat flux after ignition*)
normM=M==mdot/(1-phi) L/qo;(*steady state mass loss for non-charring*)
normtau=tau==4 alpha t/ds^2;(*dimensionless time*)
normds=ds==2 k L/(c qo);(*steady state penetration depth for non-charring*)
normd=Delta==d/ds;
normdc=Dc==dc/ds;
normTs=Ths==Ts/Tv;
normTo=Tho==To/Tv;
normgam=gam==c Tv/ L;
normdt=d==Sqrt[6 alpha t];
normtig=tig==2/3 k rho c ((Tv-To)/qo)^2;
normcg=lamg==cg/c;
normcc=lamc==cc/c;

diffeq1=Dc'[tau] == M[tau]/2;
diffeq2=M[tau](lamg(-2 + 2 Ths[tau]) + 2 phi (-lamc + lamg + lamc Tho - lamg
Ths[tau])) +  lamc phi (2 - 4 Tho + 2 Ths[tau]) Dc'[tau] + 2 lamc phi Dc[tau] Ths'[tau]
==  2/gam + (kc (1 - Ths[tau]))/(k Dc[tau]) + (eps sig Tv^4 (2 - 2 Ths[tau]^4))/(gam
qo);
diffeq3=(2 dHv M[tau])/(c Tv) == (kc ( Ths[tau]-1))/(k Dc[tau])- 2(1-Tho)/Delta[tau];
diffeq4=M[tau] + (2 Delta'[tau])/3 ==1/ Delta[tau];

icond={igDelta -> gam (1 - Tho), Mig -> 0, igDc' -> 0,
        igThs -> 1, igtau -> (2 gam^2 (1 - Tho)^2)/3};

Options[CharSolve]={
qi->50 10^3,          (*net incident heat flux w/m^2*)
cc->1000,             (*specific heat of char j/kg K*)
kc->.05,              (*thermal conductivity of char W/m K*)
phi->.05,             (*char fraction*)
rho->700      ,       (*kg/m^3*)
c->1000,              (*specific heat of virgin material  j/kg K*)
k->.08,               (*thermal conductivity of virgin material w/m K*)
Tv->700,              (*Temperature of pyrolysis K*)
L->3000 10^3,         (*heat of gasification j/kg*)
cg->1040,             (*Specific heat of volatiles j/kg K*)
kg->.03,              (*thermal conductivity of air w/m K*)
```

```
eps->.9,              (*surface emissivity*)
sig->5.865 10^-8,     (*stephen-boltzmann constant  W/m^2 K^4*)
rhoc->phi rho,              (*kg/m^3*)
dHv->L-c(Tv-To),      (*heat of vaporization j/kg*)
alpha->k/(c rho),     (*thermal diffusivity m^2/s*)
gam->c Tv/ L,         (*energy stored in solid at vaporization temp vs. heat of
gasification*)
qo->qi-eps sig Tv^4,  (*net incident heat flux w/m^2*)
Tho->To/Tv,           (*dimensionless initial temperature*)
lamc->cc/c,           (*specific heat ratio for char*)
lamg->cg/c,           (*specific heat ratio for volatiles*)
stau->.00351,         (*small time used in series analysis*)
specend->50igtau,     (*ending conditions*)
To->300               (*Initial Temperature*)};

varlist=Map[First,Options[CharSolve]];

Clear[SmallTimeSolve];
SmallTimeSolve[properties_List]:=Module[
{seriessoln,stauig,steq1v,steq2v,steq2va,steq3v,steq4v,sol1},
seriessoln={
        Ths[tau]->1+sTs (tau),Ths'[tau]->sTs,
        Dc[tau]->sDc (tau),Dc'[tau]->sDc,
        Delta[tau]->igDelta+sD (tau),Delta'[tau]->sD,
        M[tau]->Mig+sM (tau),M'[tau]->sM};

stauig=stau//.properties;

{steq1v,steq2va,steq3v,steq4v}=
        {diffeq1,diffeq2,diffeq3,diffeq4}//.Join[seriessoln,properties,icond];
steq2v=(steq2va//ExpandAll)/.{tau^_->0};
allsteqs={steq1v,steq2va,steq3v,steq4v}/.tau->stauig//N;
sol1=FindRoot[allsteqs,{sM,35,45},{sTs,1,5},{sDc,.1,.3},{sD,7,15},MaxIterations->2
50];
(seriessoln[[{1,3,5,7}]]//.Join[sol1,{tau->stauig}])/.stauig->igtau+stau
        ]
Clear[Findtau,Findtime]
Findtau[time_,opts___]:=tau/.Solve[{normtau,normds},tau,ds][[1]]/.
        t->time//.Thread[varlist->(varlist/.{opts}/.Options[CharSolve])]
Findtime[time_,opts___]:=t/.Solve[{normtau,normds},t,ds][[1]]/.
        tau->time//.Thread[varlist->(varlist/.{opts}/.Options[CharSolve])]
SetAttributes[Findtau,Listable];
```

```
SetAttributes[Findtime,Listable];

CharSolve::usage=
"CharSolve takes an optional list of property assignment rules and calculates
the solution to the charring pyrolysis case.  It returns a list with the following
structure:\n
{smtau,taubegin,tauend,Dfn[t],Dcfn[t],Ths[t],M[t]}";

Clear[CharSolve];
CharSolve[opts___]:=Module[
{initconds,icondv,initcondsv,taubegin,tauend,detemp,detemp2,ndim,useopts,
dsol,dcsol,Tssol,mdotsol,tbegin,tend,tig},

useopts=Thread[varlist->(varlist/.{opts}/.Options[CharSolve]/.{opts}/.Options[CharSo
lve])];

initconds=SmallTimeSolve[useopts];

detemp={diffeq1,diffeq2,diffeq3,diffeq4}//.useopts;
solM=Solve[detemp[[3]],M[tau] ][[1]]//Simplify;
detemp2=detemp[[{1,2,4}]]/.solM//Simplify;
initcondsv=initconds[[{1,2,3}]]//.Join[{Rule->Equal},icond,useopts];
{smtau,taubegin,tauend}={stau,igtau+stau,specend}//.Join[icond,useopts];

desol1=NDSolve[
Join[detemp2,initcondsv],
{Ths[tau],Dc[tau],Delta[tau]},
{tau,taubegin,tauend}];

Deltasol[tau_]=Delta[tau]/.desol1;
Dcsol[tau_]=Dc[tau]/.desol1;
Thssol[tau_]=Ths[tau]/.desol1;
Msol[tau_]=M[tau]//.Join[desol1//Flatten,solM];

ndim={smtau,taubegin,tauend,Deltasol[tau],Dcsol[tau],Thssol[tau],Msol[tau]}//Flatten
]

Clear[CharPlots]
CharPlots[rawsolution_List,opts___]:=Module[
{dplot,dcplot,Tsplot,mdplot,allplots,tn,tb,te,toffset,pbegin,solution},

{tn,tb,te}=rawsolution[[{1,2,3}]];
```

```
toffset=tb;
pbegin=tb-tn;
solution=rawsolution/.t->t+pbegin;
Off[InterpolatingFunction::dmwarn];
dplot=Plot[100 rawsolution[[4]],{t,0,te},
        PlotLabel->"Thermal Penetration",
        AxesLabel->{"t (s)","d (cm)"},DisplayFunction->Identity];

dcplot=Plot[1000 rawsolution[[5]],{t,0,te},
        PlotLabel->"Char Layer Thickness",
        AxesLabel->{"t (s)","dc (mm)"},DisplayFunction->Identity];

Tsplot=Plot[rawsolution[[6]],{t,0,te},
        PlotLabel->"Surface Temperature",
        AxesLabel->{"t (s)","Ts (K)"},DisplayFunction->Identity];

mdoplot=Plot[100 solution[[7]],{t,0,(te-toffset)},
        PlotLabel->"Mass Loss Rate",
        AxesLabel->{"t-tig (s)","mdot (mg/cm^2 s)"},DisplayFunction->Identity];

mdplot=Plot[100 rawsolution[[7]],{t,0,te},
        PlotLabel->"Mass Loss Rate",
        AxesLabel->{"t (s)","mdot (mg/cm^2 s)"},DisplayFunction->Identity];

On[InterpolatingFunction::dmwarn];
allplots=GraphicsArray[{{dplot,dcplot},{Tsplot,mdplot}}];

Show[Switch[(SelectPlots/.{opts}),
Thermal,dplot,
Char,dcplot,
Temp,Tsplot,
Mass,mdplot,
MassOffset,mdoplot,
_,allplots],DisplayFunction->$DisplayFunction]
        ]

Clear[CharLists]
CharLists[solution_List,opts___]:=
Module[{times,functions,fullist,selectfns},

selectfns=Switch[(SelectLists/.{opts}),
Virgin,4,
```

```
Char,5,
Temp,6,
Mass,7,
_,{4,5,6,7}];

times=solution[[{1,2,3}]];
functions=solution[[selectfns]];
fullist=Table[Thread[{t,functions}],{t,0,times[[3]]}];
If[Length[First[fullist]]>2,
Partition[Partition[#,2],Length[#]/8]&[Flatten[Transpose[fullist]]],
fullist]
]

On[General::spell1,General::spell]
```

NOMENCLATURE

A	pre-exponential factor, area
$A(t)$	coefficient in temperature profile
$B(t)$	coefficient in temperature profile
$C(t)$	coefficient in temperature profile
c	specific heat
E	internal energy
E	activation energy
ΔH_v	heat of vaporization (pyrolysis)
h	specific enthalpy
k	thermal conductivity
L	heat of gasification
M	dimensionless mass loss flux
$\dot{m}''$	mass loss flux
n	general species
p	placeholder in series solution expression
$\dot{q}''$	heat flux
$\dot{q}''_v$	heat flux conducted into the vaporization plane from the char
$\dot{q}''_k$	heat flux conducted from vaporization plane into virgin material
$\dot{q}''_0$	net surface heat flux at the onset of pyrolysis

R	gas constant
T	temperature
t	time
V	volume
v	vaporization plane velocity
x	spacial variable; used in quadratic temperature profiles
y	spacial variable, associated with linear temperature profile

α	thermal diffusivity
Δ	dimensionless distance
δ	depth of thermal penetration
ϵ	surface emissivity
σ	Stefan-Boltzmann constant
ϕ	char fraction
τ	dimensionless time
θ	dimensionless temperature
ρ	density
K	dimensionless thermal conductivity
ξ	dimensionless specific heat
γ	dimensionless heat of gasification
λ	dimensionless heat of vaporization/pyrolysis

β	ratio of heat of gasification to heat of vaporization/pyrolysis
η	dimensionless heat flux
Ω	correction factor in application of the model

Superscripts/overscripts

*	dimensionless variable, or small time increment
~	coefficient of perturbation from ignition conditions

Subscripts

ig	ignition
0	initial or ambient condition
v	virgin material, vaporization/pyrolysis condition
c	char
g	gas, volatiles
vp	vaporization plane
s	steady state

REFERENCES

1. Adamchik, V. et al., Guide to Standard Mathematica Packages Version 2.2, Wolfram Research, Inc. Champaign, IL. 1993.

2. Chen, Y., "Development of an Integral Model for Transient Pyrolysis Process and Derivation of Material Flammability Properties," Masters Thesis, Worchester Polytechnic Institute. Worchester, MA. 1991.

3. Chen, Y., Delichatsios, M. A., and Motevalli, V., " Materials Pyrolysis Properties Part I, An Integral Model For One-Dimension Transient Pyrolysis of Charring and Non-Charring Materials" Combustion Science and Technology, Vol. 88, 1992, pp. 309-328.

4. Chen, Y., Delichatsios, M. A., and Motevalli, V., "Materials Pyrolysis Properties Part II, Methodology for the Derivation of Pyrolysis Properties for Charring Materials," Combustion Science and Technology, Vol. 104, 1995. pp. 401-425.

5. Delichatsios, M. A. and de Ris, J., An Analytical Model for the Pyrolysis of Charring Materials. Factory Mutual Technical Report, 1983.

6. Di Blasi, C. "Processes of Flames Spreading over the Surface of Charring Fuels: Effects of the Solid Thickness," Combustion and Flame, Vol. 97, 1994. pp. 225-239.

7. Di Blasi, C. "Analysis of Convection and Secondary Reaction Effects Within Porous Solid Fuels Undergoing Pyrolysis." Combustion Science and Technology, Vol. 90, 1993. pp. 315-340.

8. Drysdale, D. An Introduction to Fire Dynamics, John Wiley and Sons, New York, NY. 1985. pp.174-182.

9. Flagen, R. Flame Spread Over Solid Surfaces, NBS-3-9006, National Bureau of Standards and Technology. Gaithersburg, MD. 1974.

10. Incropera, F. P., DeWitt, D. P., Fundamentals of Heat and Mass Transfer, 3rd ed., John Wiley and Sons, New York, NY. 1990. pp 259-260.

11. Iqbal, N., "Burning Rate Model for Thermoplastic Materials" Masters Thesis, University of Maryland, College Park, MD. 1993.

12. Janssens, M. L., "Fundamental Thermophysical Characteristics of Wood and their Role in Enclosure Fire Growth." Doctoral Dissertation, University of Gent (Belgium), 1991.

13. Kuo, K. K. Principles of Combusion John Wiley and Sons, New York, NY. 1986. pp. 12-21.

14. Ohlemiller, T. J., Kashiwagi, T., Werner, K., "Wood Gasification at Fire Level Heat Fluxes." Combustion and Flame, Vol. 69, 1987. pp. 155-170.

15. Özişik, M. N. Boundary Value Problems of Heat Conduction, Dover Publications, Inc. New York, NY. 1968. pp.301-338.

16. Press, W. H., et al., Numerical Recipes in C 2nd ed.,Cambridge University Press, New York. 1995. pp. 707-732.

17. Quintiere, J. G., A Semi-Quantitative Model for the Burning Rate of Solid Materials, NISTIR-4840, National Instiute of Standards and Technology, Gaithersburg, MD. June 1992.

18. Quintiere, J. G., Rhodes, B. "Fire Growth Models for Materials," Department of Fire Protection Engineering, University of Maryland, College Park, MD. 1994.

19. Suuberg, E. M., Milosavljevic, I., Lilly, W. D., Behavior of Charring Materials in Simulated Fire Environments NIST-GCR-94-645, National Instiute of Standards and Technology, Gaithersburg, MD, June 1992.

20. Tewarson, A., "Generation of Heat and Chemical Compounds in Fires." The SFPE Handbook of Fire Protection Engineering 2nd ed. P. DiNenno, ed., National Fire Protection Association, Society of Fire Protection Engineers, Boston, MA. 1995. pp. 3-53 - 3-124.

21. Wichman, I. S., Atreya, A., "A Simplified Model for the Pyrolysis of Charring Materials." Combustion and Flame Vol. 68, 1987, pp 231-247.

22. Wolfram, S. Mathematica. A System for Doing Mathematics by Computer 2nd ed., Addison Wesley Publishing Company. Reading, MA. 1991.

NIST-114
(REV. 11-94)
ADMAN 4.09

U.S. DEPARTMENT OF COMMERCE
NATIONAL INSTITUTE OF STANDARDS AND TECHNOLOGY

(ERB USE ONLY)
ERB CONTROL NUMBER | DIVISION
PUBLICATION REPORT NUMBER | CATEGORY CODE
PUBLICATION DATE | NUMBER PRINTED PAGES

MANUSCRIPT REVIEW AND APPROVAL

INSTRUCTIONS: ATTACH ORIGINAL OF THIS FORM TO ONE (1) COPY OF MANUSCRIPT AND SEND TO THE SECRETARY, APPROPRIATE EDITORIAL REVIEW BOARD.

TITLE AND SUBTITLE (CITE IN FULL)

A Burning Rate Model for Charring Materials

CONTRACT OR GRANT NUMBER: 60NANBD0120

TYPE OF REPORT AND/OR PERIOD COVERED: GCR, 1996

AUTHOR(S) (LAST NAME, FIRST INITIAL, SECOND INITIAL)

Anderson, Gregory William

PERFORMING ORGANIZATION (CHECK (X) ONE BLOCK)
- [x] NIST/GAITHERSBURG
- [ ] NIST/BOULDER
- [ ] JILA/BOULDER

LABORATORY AND DIVISION NAMES (FIRST NIST AUTHOR ONLY)

Building and Fire Research Laboratory, Fire Science Division

SPONSORING ORGANIZATION NAME AND COMPLETE ADDRESS (STREET, CITY, STATE, ZIP)

University of Maryland

PROPOSED FOR NIST PUBLICATION

- [ ] JOURNAL OF RESEARCH (NIST JRES)
- [ ] J. PHYS. & CHEM. REF. DATA (JPCRD)
- [ ] HANDBOOK (NIST HB)
- [ ] SPECIAL PUBLICATION (NIST SP)
- [ ] TECHNICAL NOTE (NIST TN)
- [ ] MONOGRAPH (NIST MN)
- [ ] NATL. STD. REF. DATA SERIES (NIST NSRDS)
- [ ] FEDERAL INF. PROCESS. STDS. (NIST FIPS)
- [ ] LIST OF PUBLICATIONS (NIST LP)
- [ ] NIST INTERAGENCY/INTERNAL REPORT (NISTIR)
- [ ] LETTER CIRCULAR
- [ ] BUILDING SCIENCE SERIES
- [ ] PRODUCT STANDARDS
- [x] OTHER NIST GCR

PROPOSED FOR NON-NIST PUBLICATION (CITE FULLY) [ ] U.S. [ ] FOREIGN

PUBLISHING MEDIUM
- [x] PAPER
- [ ] CD-ROM
- [ ] DISKETTE (SPECIFY)
- [ ] OTHER (SPECIFY)

SUPPLEMENTARY NOTES

ABSTRACT (A 2000-CHARACTER OR LESS FACTUAL SUMMARY OF MOST SIGNIFICANT INFORMATION. IF DOCUMENT INCLUDES A SIGNIFICANT BIBLIOGRAPHY OR LITERATURE SURVEY, CITE IT HERE. SPELL OUT ACRONYMS ON FIRST REFERENCE.) (CONTINUE ON SEPARATE PAGE, IF NECESSARY.)

A one dimensional model has been developed to describe the processes involved in the transient pyrolysis of a semi-infinite charring material subjected to a constant radiant heat flux. Material properties are assumed constant with respect to temperature and time. The model tracks the char layer growth, thermal penetration depth, surface temperature and mass loss rate. The integral method is described, and an example for constant surface heat flux is solved. The derivation of the model divides the material into three regions: char layer, vaporization plane, and virgin material and the equations of conservation of mass and energy are applied to each region using the integral approximation with polynomial temperature profiles. The resulting coupled, nonlinear, autonomous system of three differential equations and one algebraic equation is suitably nondimensionalized and solved using Mathematica software. The results generated by the model are compared to existing models and, a method by which effective properties for use in the model might be deduced from experimental data is suggested.

KEY WORDS (MAXIMUM OF 9; 28 CHARACTERS AND SPACES EACH; SEPARATE WITH SEMICOLONS; ALPHABETIC ORDER; CAPITALIZE ONLY PROPER NAMES)

char; fire growth; flame spread; model studies; pyrolysis

AVAILABILITY
- [x] UNLIMITED
- [ ] FOR OFFICIAL DISTRIBUTION - DO NOT RELEASE TO NTIS
- [ ] ORDER FROM SUPERINTENDENT OF DOCUMENTS, U.S. GPO, WASHINGTON, DC 20402
- [ ] ORDER FROM NTIS, SPRINGFIELD, VA 22161

NOTE TO AUTHOR(S): IF YOU DO NOT WISH THIS MANUSCRIPT ANNOUNCED BEFORE PUBLICATION, PLEASE CHECK HERE. [ ]

ELECTRONIC INFORMS